R. & M. No. 3622

MINISTRY OF TECHNOLOGY

AERONAUTICAL RESEARCH COUNCIL
REPORTS AND MEMORANDA

A Three-Parameter Family of Mean Velocity Profiles for Incompressible Turbulent Boundary Layers with Distributed Suction and Small Pressure Gradient

By B. G. J. THOMPSON
Engineering Department, University of Cambridge

1970

PRICE £1 4*s* 0*d* [£1·20] NET

A Three-Parameter Family of Mean Velocity Profiles for Incompressible Turbulent Boundary Layers with Distributed Suction and Small Pressure Gradient

By B. G. J. THOMPSON

Reports and Memoranda No. 3622**
April, 1969

Summary.

The earlier profile family and skin-friction law for impermeable surfaces[18] is extended to account for the effects of distributed suction. It has been tentatively assumed that the nylon suction surface used by Sarnecki[14] is effectively smooth and continuously permeable as required by this simple approach. Accurate skin friction values and reasonable profile shapes are predicted for zero pressure-gradient layers on this surface, provided that reversion to laminar flow has not started.

Charts are presented from which profile shapes can be calculated, using the basic relationships given in the text, once values of H, R_θ and $\frac{v_s}{U_1}$ are specified. c_f values can be obtained directly from these charts.

Further improvements in profile shape would be expected if a blending region were incorporated.

LIST OF CONTENTS

*Now at the National Physical Laboratory, Teddington.

**Replaces A.R.C. 31 145.

---

1. *Introduction.*

The direct effects of distributed suction on the value of c_f for given values of H and R_θ must be accounted for in any accurate calculation method as if the usual solid surface relationships are used the predictions for $R_\theta(x)$ development, even in zero pressure-gradient layers, are poor as Fig. 4 shows.

A relationship of the form

$$c_f = f\left(H, R_\theta, \frac{v_s}{U_1}\right), \tag{1}$$

is derived from a new family of mean velocity profiles which use a generalised form of the intermittency model found previously to give good results for layers without transpiration (*see* Ref. 18). The relationship

(1) is presented graphically and as an analytic approximation.

As a large number of factors may influence the velocity profile with suction, it is important to notice that the present simple treatment is restricted to settled conditions where the flow accelerations have negligible effects upon the wall region behaviour and to suction surfaces with a sufficiently fine porosity structure that they impose no roughness scale or discrete sink effects on the inner region.

Discussion of the results of comparisons of predicted profiles with experiment and of calculations of momentum thickness development are given and it is shown that the present use of the data of Sarnecki[14], measured in layers on a nylon suction surface, is unlikely to be greatly affected by roughness.

Other difficulties remain and are discussed, notably the uncertainty regarding the range of pressure gradient and upstream conditions for which the present simple assumptions are likely to hold.

2. *Review of Suction Measurements.*

Kay[8] and later Dutton[4] showed the results of their zero pressure-gradient experiments with suction. Unfortunately, although the sintered bronze surface used by Kay is probably very close to the ideal of continuous permeability no complete developments of turbulent layers with suction were shown. Dutton's experiments covered a large number of complete developments but his velocity profiles were usually defined by only a few points obtained from pitot combs and were not thought suitable for developing a profile family especially as an inner region correlation would be difficult to obtain.

Black and Sarnecki[1] used their own results to find a tentative inner region correlation for the bilog. law, but this work has been superseded by the later experiments of Sarnecki[14] which were very detailed*. These measurements were made in zero pressure gradient with nominally uniform suction rate applied through a surface of perforated brass sheet (0·02 in. diameter holes at 0·04 in. centres in a hexagonal array) supported at $\frac{5}{8}$ in. intervals along the chord by $\frac{1}{8}$ in. wide wooden strips, and covered with a variety of materials to smooth out the suction distribution.

These layers will be mentioned frequently in the remainder of this paper and the notation used (due to Sarnecki) is explained below.

Each layer is denoted by a single letter referring to the type of suction surface:

N—brass sheet covered by a single sheet of calendered nylon (100 threads to the inch),

B—as above but with a single layer of blotting paper interposed between the perforated brass and the nylon.

P—uncovered perforated brass sheet.

This letter is followed by three numbers denoting the suction rate $\frac{v_s}{U_1}$ multiplied by 10^5.

Profiles are denoted by the layer code preceded by the number (x) of inches the measuring station was downstream of the beginning of the suction surface.

For example, profile 20N098 is measured at a distance of 20 ins. downstream of the start of the suction, on the nylon surface at a suction rate of 0·00098.

Layers N098, N246, N443, N688, B401, and P404 are considered with profiles at $x = 10$, 20, 30, 40 and 50 ins. and the asymptotic layer on the nylon surface (N374) measured at 5 in. intervals between 5 ins. and 55 ins. Figs. 4 and 5 show the R_θ and H developments on the nylon surface.

Tennekes[16] measured several layers on a filter paper suction surface. Unfortunately, his profiles were obtained using a round pitot of rather large diameter (0·032 ins.) in layers whose thickness varied from 0·28 to 0·6 ins. Very few points were measured in the inner regions and most of these are affected considerably by the large pitot displacement effects which Tennekes ignored in his analysis. This data has not been considered further in view of these uncertainties and Tennekes' profile analysis is also thought to offer no advantages over the present approach at least until it is re-examined on the basis of more reliable measurements.

---

*Tables of velocity profile data were kindly supplied by Sarnecki and have been reprocessed by the present author.

Sarnecki's profiles were obtained using flattened pitots with mouths of overall depth 0·01 ins. Uncorrected data has been used here but it is acknowledged that in the thinner layers (N688 especially) corrections for displacement should have been applied although some uncertainty exists regarding their exact form for flattened (as opposed to round) pitots.

Finally, measurements in nominally zero pressure gradients on a sintered metal surface of average pore size 0·004 in., have been made by Favre, Dumas and Verollet[5] and further details are given in Favre, Dumas, Verollet and Coantic[6]. Their individual velocity profiles obtained with hot-wires appear to agree very satisfactorily with the predicted sublayer profiles but their developments of H and R_θ are very scattered and appear, at the stronger suction rates, to be affected by adverse pressure gradients which are not accurately specified, also for any given layer, only one velocity profile is shown.

The main interest of these experiments lies in the measurements of turbulence quantities that are shown and their shear stress profiles are particularly useful as they give some guide (*see* later) to the length of suction surface required for a layer to recover from the sudden onset of the suction.

Measurements of velocity profiles in layers developing in adverse pressure gradients on the sucked upper surfaces of aerofoils have been made by the present author[19]. Comparisons between the new family and these measured profiles are shown and discussed in that paper and are mentioned only briefly here, in Section 4.5.

3. *The Profile Family.*

3.1. *The Intermittency Model.*

For turbulent layers without transpiration Thompson[18] showed that accurate velocity profiles could be built up on the basis of the intermittency model proposed by Sarnecki[14], in which

$$u = u_t \gamma_s + (1-\gamma_s) U_1 , \tag{2}$$

where u_t is the velocity within the 'turbulent' fluid, taken as a mean over 'time turbulent'. It was given by the inner region velocity distribution extended throughout the layer. The particular form of wall profile used in the profile family was defined numerically and shown in Fig. 4 of Thompson[18]. That is,

$$\text{in the sublayer, } w = u_t = \frac{U_\tau{}^2 y}{\nu}, \tag{3}$$

$$\text{in the fully turbulent region } v = u_t = U_\tau \left[5{\cdot}4 + 5{\cdot}5 \log_{10} \frac{U_\tau y}{\nu} \right]. \tag{4}$$

A blending region profile was obtained from the analysis of van Driest[3] with the choice of mixing length constant $\kappa = 0{\cdot}419$, and damping coefficient $\alpha_0 = 0{\cdot}0379$ compatible with the chosen log. law constants as the expression (4) defines the asymptotic behaviour of the velocity distribution for large values of $\frac{U_\tau y}{\nu}$.

w, v are used throughout where it is required to distinguish between the sublayer and fully turbulent parts of the u_t profile.

Sarnecki analysed many measured velocity profiles on solid walls for the intermittency γ_s, using (2) in the form

$$\gamma_s = \frac{U_1 - u}{U_1 - u_t}. \tag{5}$$

He found that if γ_s was normalised with respect to the height $y = \delta_s/2$ at which $\gamma_s = 0{\cdot}5$ then a single correlation curve fitted the data satisfactorily.

Hence, the profile family was constructed on the basis of the above assumptions for u_t and the universal

curve of

$$\gamma_s = \gamma_s\left(\frac{y}{\delta_s}\right), \quad \text{only} \tag{6}$$

shown in Fig. 1.

As shown in the earlier report, the 'intermittency' γ_s is somewhat different from the measured intermittency distribution, for which $\gamma = 0{\cdot}5$ lies usually in the range $0{\cdot}8 > y/\delta > 0{\cdot}6$ depending upon the upstream history of the boundary layer. However, this does not detract from the usefulness of the present approach which usually gives detailed profile shapes that are superior to those of the 'wake' model of Coles[2], for example. Furthermore Black and Sarnecki[1] showed that the wake model was difficult to extend to the conditions of distributed suction or injection.

3.2. *The Turbulent Fluid Velocity Distribution with Suction.*

With suction, the inner region velocity distributions corresponding to (3) and (4) are

$$w = u_t = \frac{U_\tau^2}{v_s}\left[1 - \exp\frac{-v_s y}{\nu}\right] \text{for } y \leqslant y_a, \tag{7}$$

$$\text{and } v = u_t = \frac{U_\tau^2}{v_s} - \frac{1}{v_s}\left[\frac{v_s}{2\kappa}\log_e\frac{y}{d}\right]^2 \text{for } d \geqslant y \geqslant y_a \tag{8}$$

A blending region analysis using van Driest's approach was suggested by Sarnecki but has not been used in the present profile family although preliminary calculations have been made suggesting that the use of a blending profile would significantly improve agreement with experiment at moderate suction rates (*see* Section 4.4).

The bilogarithmic expression (8) has been discussed extensively by Black and Sarnecki[1] and, for suction in particular, by Sarnecki[14].

From (8) it can be seen that the bilog. law predicts a maximum value of velocity

$$u_t = \frac{U_\tau^2}{v_s} \tag{9}$$

at a height $y = d$.

Above this the velocity gradient $\dfrac{\partial u}{\partial y}$ becomes negative and so this branch of the bilog. curve is physically unacceptable for u_t. In the absence of further knowledge the simplest possible assumption is made that

$$u_t = \frac{U_\tau^2}{v_s} \text{ for all } y \geqslant d, \tag{10}$$

in the new profile family, although this is not strictly justifiable as the bilog. profile is not consistent with the assumption at fully turbulent flow as y approaches d, as from (8) it can be shown that

$$\frac{\tau_{\text{VISC.}}}{\tau_{\text{TOTAL}}} = \frac{-2\nu}{v_s y}\left[\log_e\frac{y}{d}\right]^{-1} \to \infty \text{ as } y \to d \tag{11}$$

The bilog. law can also be written as

$$u_t = U_\tau\left[\frac{U_\tau}{v_s}(1-\lambda^2) + \frac{\lambda}{\kappa}\log_e\frac{U_\tau y}{\nu} - \frac{1}{4\kappa^2}\frac{v_s}{U_\tau}\left\{\log_e\frac{U_\tau y}{\nu}\right\}^2\right] \tag{12}$$

where the parameter d is now replaced by

$$\lambda = \frac{1}{2\kappa}\frac{v_s}{U_\tau}\log_e\frac{U_\tau d}{\nu}, \tag{13}$$

and is a function only of $\frac{v_s}{U_\tau}$, for the ideal smooth continuously permeable suction surface.

A further rearrangement of the bilog. law is useful,

$$\frac{u}{U_1} + Y_s^2 = (p^2{}_s - n^2{}_s) + 2n_s Y_s, \tag{14}$$

where

$$Y_s = \frac{1}{2\kappa}\sqrt{\frac{v_s}{U_1}}\log_e\frac{U_1 y}{\nu}, \tag{15}$$

$$n_s = \frac{1}{2\kappa}\sqrt{\frac{v_s}{U_1}}\log_e\frac{U_1 d}{\nu}, \tag{16}$$

and

$$p_s^2 = \frac{U_\tau^2}{v_s U_1}. \tag{17}$$

Consequently if $\frac{u}{U_1} + Y_s^2$ is plotted against Y_s, a linear portion appears and from its slope and intercept c_f and d can be found, and hence the value of λ also, from (13).

With the assumption that $\kappa = 0{\cdot}419$ irrespective of transpiration rate, Sarnecki[14] analysed his own zero pressure-gradient suction measurements and obtained the results shown in Fig. 2. The corresponding γ_s distributions were presented for small suction rates $\frac{v_s}{U_1} \leqslant 0{\cdot}004$, approximately and as Fig. 1 shows they could be adequately represented by the mean curve used in the profile family for zero transpiration.

Although straight lines could still be found (to within experimental accuracy) on the bilog. plots for profiles at larger suction rates the values did not follow the trend at lower values of $\frac{v_s}{U_\tau}$ and spread widely. The associated γ_s distributions departed considerably from the 'universal' curve previously used. These difficulties were resolved as described in the next Section.

3.3. *Profile Assumptions at Large Suction Rates.*

The co-ordinate $\frac{U_\tau y_a}{\nu}$ of the intersection between the sublayer and bilog. profiles can be found from (7) and (12) once the variation of λ with $\frac{v_s}{U_\tau}$ is assumed. The variations of $\frac{U_\tau y_a}{\nu}$ with $\frac{v_s}{U_\tau}$ are shown in Fig. 13 for both the λ curve used in the new profile family and for Sarnecki's λ curve.

The sublayer and bilog. curves become tangential at a limiting value of $\frac{v_s}{U_\tau}$ beyond which no real intersections are found and the sublayer profile must then be assumed to occupy the whole of the inner region and hence (7) must be used, in the absence of further information, to describe the whole of the u_t distribution.

The intermittency $\gamma_s\left(\frac{y}{\delta_s}\right)$ is now very close to the universal curve as Fig. 1 shows for a profile measured

by Favre *et al*[6] at the high suction rate of $\frac{v_s}{U_1} = 0{\cdot}0153$. Consequently the intermittency model predicts the overall profile shape very accurately for this profile, as seen in Fig. 3, where the comparison with experiment is made on the basis of the c_f value appropriate to the measured sublayer.

3.4. *The Numerical Procedure for Calculating Velocity Profiles and Skin-Friction Values.*

Once the variation of λ with $\frac{v_s}{U_\tau}$ had been assumed (*see* next Section) an AUTOCODE programme was used to evaluate the corresponding variation of $\frac{U_\tau y_a}{\nu}$ for $\frac{v_s}{U_\tau}$ values up to the limiting value which was found by trial and error. The values* of $\frac{v_s}{U_\tau}$, λ and $\frac{U_\tau y_a}{\nu}$ were then used, together with the table of γ_s *versus* $\frac{y}{\delta_s}$ given in Thompson[18], in a second programme which calculated velocity profiles for desired values of H, R_θ and $\frac{v_s}{U_1}$.

The procedure took the following form:

Profiles can be calculated using equations (2), (7), (10) and (12) subject to the conditions mentioned in Sections 3.2 and 3.3, provided values of $\frac{v_s}{U_1}$, c_f and $R_{\delta_s}\left(=\frac{U_1\delta_s}{\nu}\right)$ are chosen. Therefore, initial guessed values of $c_f\,(=c_{f_1})$ and of $R_{\delta_s}\,(=R_{\delta_{s1}})$ were fed in to the computer as well as the value of $\frac{v_s}{U_1}$; $\frac{v_s}{U_\tau}$ was calculated and, if less than the limiting value for which the bilog. profile vanishes, values of λ, $\frac{U_\tau y_a}{\nu}$ and, from equation (13), of $\frac{U_\tau d}{\nu}$ were found.

The velocity distribution

$$\frac{u}{U_1} = f\left(\frac{y}{\delta_s}, c_f, R_{\delta_s}, \frac{v_s}{U_1}\right), \tag{18}$$

was then calculated for selected values of $\frac{y}{\delta_s}$ using the tabulated intermittency distribution and equation (2).

Integration, using the trapezium rule, gave $\frac{\delta^*}{\delta_s}$ and $\frac{\theta}{\delta_s}$ from which H and R_θ were found and compared with the desired values. New estimates for $c_f\,(=c_{f_2})$ and $R_{\delta_s}\,(=R_{\delta_{s2}})$ were obtained from†,

$$c_{f_2} = c_{f_1} \times \left[\frac{H\ \text{CALC.}}{H\ \text{DESIRED}}\right], \tag{19}$$

---

*Table 2 gives the values used in the profile family presented here.

†The local contours of c_f, R_{δ_s} in the H, R_θ plane were defined in another iteration procedure, by calculating profiles with first c_f and then R_{δ_s} varied from the previous estimates by a small percentage. This gave an approximate (linearized) relationship from which the next estimate could be obtained by simple geometrical considerations.

and,
$$R_{\delta_{s2}} = R_{\delta_{s1}} \times \left[\frac{R_\theta \text{ DESIRED}}{R_\theta \text{ CALC.}} \right] \tag{20}$$

This process was repeated until the values of H and R_θ had converged to within $\pm\frac{1}{2}$ per cent of the desired input values. The output was given in the form of H, R_θ, c_f and $\frac{v_s}{U_1}$ values together with the velocity profile tabulated as $\frac{u}{U_1}$ *versus* $\frac{y}{\theta}$ for comparison with experiment. A similar programme can be used for profiles without transpiration but near the limiting condition (at low H values) of

$$u_t = U_1, \text{ at } y = \delta_s, \tag{21}$$

the straightforward profile model breaks down and the charts presented in Thompson[18] have more plausibility as a velocity defect assumption is used together with a revised definition of boundary layer thickness (δ_1) to improve the outer region. No attempt is made in the present Report to incorporate this revised outer region in profiles with suction, and the limiting curve corresponding to (21) is shown on each chart.

The initial estimates of c_f, R_{δ_s} for any calculation of profiles from the new family can be easily found by using Figs. 14 and 25 which show the relationships

$$c_f = c_f\left(H, R_\theta, \frac{v_s}{U_1}\right), \tag{22}$$

and
$$R_{\delta_s} = R_{\delta_s}\left(H, R_\theta, \frac{v_s}{U_1}\right), \tag{23}$$

for values of suction rate $\frac{v_s}{U_1} = 0$, 0·001, 0·002, 0·005, 0·010, and 0·015. Typical variations of c_f with $\frac{v_s}{U_1}$ for given values of H and R_θ are shown in Fig. 26, where it is apparent that skin-friction values can be found for intermediate suction rates quite accurately by cross-plotting values from the charts presented here. Using these values the programmes require usually only one iteration to converge to within $\pm\frac{1}{2}$ per cent of H and R_θ. Each profile calculation takes about 0·2 secs. computing time on a machine of $5\mu S$ multiplying time.

These charts were constructed because the number of iterations became very large if the initial estimates of c_f or R_{δ_s} were very inaccurate and, even with their aid, the double-valued nature of the profile family (with respect to H) near the limit (21) means that difficulties can occur using simple iteration procedures such as (19) and (20). The variation of c_f near the limit is shown typically for larger suction rates, in Fig. 27. The calculations carried out by the author have been restricted entirely to the main branch of these curves. The second branch in which H rises $\left(\text{at given values of } R_\theta \text{ and } \frac{v_s}{U_1}\right)$ with rising c_f is indicated in Figs. 17, 18 and 19 by using dashes instead of full lines for the c_f contours near the limiting value.

3.5. *The Determination of the λ Curve from Sarnecki's Data.*

The curve suggested by Sarnecki[14] and shown in Fig. 2 was used initially to calculate profile shapes and c_f values for the layers on the nylon surface. The agreement with measured profiles was generally very good except for the larger suction rates where it was thought that laminar reversion had begun, but the skin-friction values at low suction rates $\frac{v_s}{U_1} \leqslant 0{\cdot}002$ were unacceptably small and less (at given values of

H and R_θ) than those predicted for solid surfaces. This resulted in poor predictions for the R_θ growth in layers N098 and N246.

Stevenson's λ variation (also shown in Fig. 2) was then used and resulted in poor predictions for profile shape especially in the inner region. The c_f values were much larger than those calculated from the measured momentum developments in Sarnecki's layers except for the very small suction rates $\frac{v_s}{U_1} \leqslant 0{\cdot}001$ approximately.

The spread of the data points in Fig. 2 is quite considerable and meant that it was not immediately obvious how the λ curve should be chosen in order to combine acceptable agreement with profile shapes whilst retaining skin-friction values that resulted in good predictions for $R_\theta(x)$ in these layers, if indeed this was possible without further complicating the basic model.

The best compromise could not be found by considering individual profiles because of uncertainties as to local values of suction rate and pressure gradient in these experiments. Mean values over the whole of each development are, however, known accurately and profiles at several stations were considered. However, it was by no means certain that individual layers could be fitted accurately as their variations might not combine to give the overall smooth variation with respect to $\frac{v_s}{U_1}$ that is necessary for the final correlation. Consequently, it was necessary to proceed by trial and error, assuming a succession of smooth λ curves until the best overall result for profile shape and skin-friction was obtained. At the third attempt a suitable curve was found and is shown in Fig. 2. This has been used as the basis of the profile comparisons shown in Figs. 6 to 12, and of the relationships for c_f and R_{δ_s} described in the previous section.

3.6. *The Comparisons of Predicted Profiles with Experiment.*

In order to obtain the good predictions for $R_\theta(x)$ shown in Fig. 4, it was necessary to accept the level of disagreement with measured profiles shown for layer N246 in Fig. 7 and for layer N374 in Fig. 8. The departures from profiles 30N443, 50N443 in Fig. 11, and from 10N688, 30N688 in Fig. 12 are due to the use of H values as a basis for comparison near to the limits of the family when it becomes double valued with respect to H for large suction rates. This is shown in Fig. 27 for the skin-friction relationship.

If the boundary layer thickness had been used as a parameter then the agreement would have been much improved. It is not certain that a blending region profile would improve agreement with experiment in these conditions where reversion to laminar flow is indicated by the rising H values shown in Fig. 5. It is likely that the other branch of the family in which

$$\left[\frac{\partial H}{\partial c_f}\right]_{R_\theta, \frac{v_s}{U_1}} > 0, \tag{24}$$

could be used* at least when H is rising in conditions of uniform suction and zero pressure gradient.

The absence of a blending region seems to be the reason for the disagreement at the lower suction rates for the layers with these low Reynolds numbers, except possibly where the layer is settling down after the start of the suction, as in the case of 10N098 and 10N246.

Profiles in layer B401 (*see* Fig. 9) are very well predicted but it is difficult to estimate the range of surface conditions for which the use of the present λ curve will result in accurate profiles. However, the calculations for layer P404 (*see* Fig. 10) shows, as expected, that the present family is inaccurate for layers on surfaces where the suction is applied through discrete perforations.

For comparison with the new family, calculated profiles are shown in Figs. 6 to 11 for which the λ assumption of Stevenson[15] has been used. The poorer agreement is immediately apparent.

---

*The iteration relationships (19) and (20) need to be changed as they assume that $\frac{\partial H}{\partial c_f} \leqslant 0$.

3.7. *The Skin-Friction Relationship.*

3.7.1. *The use of the graphical presentation in calculations of momentum thickness development.* The charts shown here as Figs. 14 to 19, and described in Section 3.4 have been used together with the measured H development and the momentum integral equation for two-dimensional mean flow, to give the good predictions of $R_\theta(x)$ shown in Fig. 4. The use of the solid surface c_f law yields comparatively poor results.

3.7.2. *The analytic approximation.* The momentum calculations shown in Thompson[17,19] make use of an analytic approximation to the charts for $\frac{v_s}{U_1} = 0$, 0·005 and 0·010, with a linear interpolation or extrapolation to give the c_f values at other suction rates. The analytic expressions are due to Krishnamurthy[9] and are summarized in Appendix 1.

This approximation is compared with the exact relationship in Figs. 14, 17 and 18. The contours for c_f are well represented for $\frac{v_s}{U_1} = 0$ and 0·01 but at low values of H the accuracy is less satisfactory at the suction rate of 0·005.

Fig. 26 indicates that the linear interpolation overestimates c_f values by 10 to 20 per cent in the range $0{\cdot}002 \leqslant \frac{v_s}{U_1} \leqslant 0{\cdot}004$. This has affected the predictions for $R_\theta(x)$ in layers D, F, and J in Thompson[19].

In retrospect it appears that a chart for $\frac{v_s}{U_1} = 0{\cdot}002$ or 0·003 should have been approximated by an analytic expression. Linear interpolation with respect to suction rate would then be sufficiently accurate. However, the relatively crude nature of the present profile assumptions may not warrant this additional work and it is thought that it is preferable to incorporate a blending profile first.

4. *Discussion.*

4.1. *Roughness and Non-Homogenity of Suction Surfaces.*

Solid surfaces are aerodynamically smooth when the height (k) of the equivalent sand roughness is such that $\frac{U_\tau k}{\nu} \leqslant 5$, in zero pressure gradient conditions. Now, the sublayer 'thickness' (y_a) is such that $\frac{U_\tau y_a}{\nu} = 11{\cdot}2$ with the present choice of inner region constants, and so it seems reasonable to assume that if $k \leqslant 0{\cdot}5\, y_a$ a suction surface will also behave in the ideal aerodynamically smooth manner. If k is interpreted also as the average repeat length of the discrete pore structure of any real surface, the same criterion may also be used for homogeneity of section.

Using the curve of $\frac{U_\tau y_a}{\nu}$ *vers* $\frac{v_s}{U_\tau}$ (shown in Fig. 13) values of y_a have been calculated (*see* Table 1) for Sarnecki's suction layers on nylon surface. U_τ was obtained from the skin-friction values found by using the measured momentum growth. From Section 2, it is estimated that $0{\cdot}005 \leqslant k \leqslant 0{\cdot}01$ in. for the nylon surface and Table 1 shows that if the lower value of k is used then only layer N098 is likely to be affected by 'roughness'. However, if the upper limit is correct then this surface may not be ideal aerodynamically unless $\frac{v_s}{U_1} > 0{\cdot}004$.

This relatively crude treatment suggests that the effects of surface structure in Sarnecki's nylon layers are not very significant as the surface scale length is usually less than the sublayer thickness. Some uncertainty will remain, however, until new measurements are made in zero pressure gradient using a finer grain surface.

McQuaid[12], when describing his injection experiments, has considered surface conditions in greater

detail and showed that the porous-plastic suction-surface material*, used also in the present author's experiments on suction aerofoils[19], has a porosity scale of the order of 0·001 in. and should provide an ideal transpiration surface, at least for the present range of zero pressure-gradient conditions.

4.2. *Blockage to Suction Flow due to the Structure Underlying the Actual Suction Surface.*

The surface tube traverses made by the present author on the porous-plastic suction surface showed that the spanwise strips supporting the surface at $\frac{1}{2}$ in. intervals along the chord were each obstructing the suction flow locally. The construction of the surfaces used by Dutton[4] and by Sarnecki[14] are very similar in this respect and their zero pressure-gradient results may be affected by these periodic dips in $\frac{v_s}{U_1}$. Head[7] showed that a given overall suction flow reduced the momentum thickness of laminar layers less effectively if it was applied through discrete strips rather than distributed uniformly along the whole surface.

Therefore if the momentum development of a layer is found by measuring only the usual small number of profiles, the skin-friction values calculated from the momentum balance will be larger for a given average suction rate. Also, in a region where there is an appreciable gradient of suction velocity along the surface, the first order boundary-layer approximations may no longer apply and the usual inner region treatments may not be justified.

In any analysis of present data these uncertainties must be ignored although the systematic influence on the inner region correlations might be significant if in a given layer all profiles had been measured at x-positions which bore a fixed relationship to the positions of the supporting strips and hence were in the same phase relationship to the periodic variations of suction rate in the x-direction. It is probable that this was the case with Sarnecki's measurements.

4.3 *The Behaviour of the Boundary Layer Immediately Following the Start of the Suction.*

A finite distance downstream of the leading edge of the suction surface is required before the sucked layer reaches a settled state to which the present simple profile assumptions can be expected to apply. It is not possible with our present knowledge to predict the length of the settling region, but a rough guide can be obtained from the behaviour of the shear-stress distributions measured by Favre *et al*[5]. Considering only the layer for $\frac{v_s}{U_1} = 0{\cdot}0025$ and comparing these results in Fig. 28 with shear stresses calculated (by means of an AUTOCODE programme) from the measured velocities in layer N246 using the equations of motion it is found that the shear-stress variation in the inner region takes about 30 mean boundary layer thicknesses (δ) to settle to the distribution

$$\frac{\tau}{\rho} = \frac{\tau_0}{\rho} + v_0 u, \tag{25}$$

appropriate to small rates of x-variation $\frac{\partial v_0}{\partial x} \approx \frac{\partial \tau_0}{\partial x} \approx 0$, as assumed in the present inner region analysis. Favre's measurements show minima in stress for stations closer to the start of the suction.

The disagreement between the present family and the measured profiles 10N098 (Fig. 6) and 10N246 (Fig. 7) may therefore be due to the incompletely settled nature of these layers at these stations. The remaining profiles should not suffer from this uncertainty.

4.4. *The Use of a Blending Region Profile.*

The straight lines drawn on the bilog. plots of Sarnecki's profiles were fitted to the measurements

*Vyon, manufactured by Porous Plastics Ltd., Dagenham Dock, Essex.

usually over the range

$$40 \leqslant \frac{U_\tau y}{\nu} \leqslant 150, \text{ for } 0{\cdot}00098 \leqslant \frac{v_s}{U_1} \leqslant 0{\cdot}00443 \tag{26}$$

Now from Section 3.2,

$$\frac{\tau_{\text{VISC.}}}{\tau_{\text{TOTAL}}} = -2\frac{\nu}{v_s y}\left[\log_e \frac{y}{d}\right]^{-1}, \tag{11}$$

$$= \frac{U_\tau y}{\nu}\left[\kappa\lambda - \tfrac{1}{2}\frac{v_s}{U_\tau}\log_e \frac{U_\tau y}{\nu}\right], \tag{27}$$

from equation (13).

Equation (27) has been used to calculate this shear-stress ratio for $\frac{v_s}{U_\tau} = 0{\cdot}01$, $0{\cdot}06$ and $0{\cdot}07$ as shown in Fig. 29.

This ratio has also been calculated directly from the measured velocity profiles in layers N246 and N374, using the boundary-layer equations. Typical results are shown in the same figure.

It is seen that the ratio is generally 5 per cent greater in the bilog. region if $\frac{v_s}{U_\tau} \geqslant 0{\cdot}05$. Now in the case of zero transpiration the outer limit of the blending region is usually assumed to be at about $\frac{U_\tau y}{\nu} = 50$, which corresponds to a stress ratio of $0{\cdot}05$. The above results show that it is necessary to incorporate a blending region in the profile family if profiles in layers N374, N443, and N246 are to be accurately represented, thereby removing most of the discrepancies in Figs. 8, 11 and 7.

The blending region model proposed by van Driest[3] assumes an exponential decrease of the mixing length constant (κ) to zero at the wall. At large values of $\frac{U_\tau y}{\nu}$ it reduces for zero transpiration to the usual semilogarithmic fully turbulent form, whilst at the surface it reduces to the usual linear sublayer profile.

The damping factor (α) can be assumed to depend only upon $\frac{v_s}{U_\tau}$ and a complete description of inner regions with suction can be obtained in principle, if the correlation of $\frac{\alpha}{\alpha_0}$ against $\frac{v_s}{U_\tau}$ is found from experiment, where α_0 is the value for zero transpiration.

There was insufficient time available for the present author completely to reanalyse Sarnecki's profile data but some encouraging preliminary results have been obtained using an AUTOCODE programme and some examples are shown here in Fig. 30 for layers N098 and N443. The previously accepted value for $\kappa = 0{\cdot}419$ has been used together with $\alpha_0 = 0{\cdot}0379$ which leads to the semilogarithmic form (4) at large values of $\frac{U_\tau y}{\nu}$, in the absence of transpiration.

4.5. *The Effects of Pressure Gradients.*

For a given surface shear the suction lowers the stress level in the inner region compared with zero transpiration conditions. The effects of a given adverse pressure gradient are therefore to cause a proportionately larger departure of the local shear stress, from that obtaining without pressure gradient, than would occur in the absence of suction.

Consequently, we must replace the pressure gradient parameter $\Delta = \frac{\nu}{U_\tau^3}\frac{1}{\rho}\frac{dp}{dx}$ used for solid walls, by

a parameter such as $\Delta_i = \frac{\nu}{(U_\tau^2 + v_0\bar{u})^{\frac{3}{2}}} \frac{1}{\rho}\frac{dp}{dx}$ as suggested by McQuaid[11], where $(U_\tau^2 + v_0\bar{u})$ is the measure of the local stress in the inner region, $\bar{u}$ being a representative mean velocity in this part of the layer. McQuaid showed that his injection profiles agreed with the zero pressure gradient assumptions provided that Δ_i lay between the same numerical limiting values as found previously (for Δ) for solid surface profiles by Patel[13]; namely $|\Delta| \leqslant 0{\cdot}0034$.

The local skin-friction and pressure-gradient values appropriate to the profiles measured in the suction aerofoil layers (Thompson[19]) are not known accurately enough to estimate the corresponding limits to Δ_i for suction. Additional measurements including the direct determination of skin friction would be required before such limits could be found.

The adverse pressure gradients in these aerofoil layers result in considerable departures from the simple family presented here but, at present, there is no satisfactory description of the inner region on smooth solid walls once large pressure gradients arise (*see* Patel[13]) and so it is probable that this simpler problem must be solved before progress can be made with a general description of profiles with combined suction and adverse pressure gradient.

4.6. *The Use of the Sublayer Velocity Distribution for u_τ.*

Using the sublayer profile as the assumed velocity distribution within the 'turbulent fluid' (or more correctly the vorticity bearing fluid) for $\frac{v_s}{U_\tau}$ greater than a limiting value (0·0717 in the case of the present profile family) can be justified as being compatible with a plausible picture of the boundary layer reverting to laminar flow in zero pressure gradient with a constant suction rate along the surface. The smaller turbulent motions in the rotational fluid will decay first as their Reynolds numbers are smaller than those associated with the scales responsible for the intermittent nature of the flow. The difference in velocity between the viscous profile and the freestream will then gradually fall to zero as the unsteady 'laminar' flow settles to the asymptotic laminar profile where $\frac{U_\tau^2}{v_s U_1} = 1, H = 2$ and $\frac{v_s\theta}{\nu} = \frac{1}{2}$.

This process seems to be occurring in some of the measured layers at these low Reynolds numbers. However, it is not certain that, if the upstream conditions (length of solid surface preceding suction, or a region of adverse pressure gradient) were such as to raise the Reynolds numbers considerably ($R_\theta \approx 10^4$ instead of 10^2 to 10^3 as at present), the present model would be suitable even if the direct effects of the upstream history had apparently disappeared, sufficiently far from the start of the suction.

It may be that layers on a given suction surface cannot be expected to settle down after the initial disturbances creating the high Reynolds numbers until the local Reynolds number of the sucked layer has fallen to the present measured range. That is, we may find that the inner regions are influenced by the acceleration terms and are not solely dependent upon $\frac{v_s}{U_\tau}$. It will be necessary therefore to correlate an 'effective λ' against $\Delta_2 = \frac{\nu}{U_\tau^3}\frac{1}{\rho}\frac{d\tau_0}{dx}$ (say) or against a suitable Reynolds number as fully turbulent inner regions may well occur when $\frac{v_s}{U_\tau}$ is greater than the present limiting values.

Measurements over a much larger range of starting values of H and R_θ are needed than are at present available.

4.7. *Comparison with the Proposals of Tennekes and of Stevenson.*

The profile data of Tennekes[16] has been briefly reviewed in Section 2 and appears to be unsuitable for accurate inner region analyses. Hence his proposed inner profile which rejects the mixing length approach in favour of a similarity argument cannot be considered as satisfactorily established on the basis of this data.

Tennekes' approach avoids the strong dependency of the bilog. profile on the exact assumption made for the mixing length constant (κ) (*see* McQuaid[12]) but suffers from the disadvantage that it does not

provide a single continuous description of inner profiles at all transpiration rates.

The inner region proposed by Stevenson[15] is a special case of the bilog. profile, having a particularly simple λ variation. However, the profile comparisons in Figs. 6 to 11, show that it leads to poor results on continuously permeable suction surfaces and has been rejected in favour of the λ assumption used in the new profile family.

5. *Conclusions.*

(i) The new family of profiles predicts the overall shapes of measured velocity distributions reasonably well but would be improved by incorporating a blending region for the low Reynolds numbers considered here.

(ii) The skin-friction law results in good predictions of momentum thickness development for layers with zero pressure gradient on the nylon surface used by Sarnecki. The agreement is generally poor if the solid surface skin-friction law is used instead. Therefore the full relationship must be used in boundary layer calculations.

(iii) The analytic approximation to the skin-friction law proposed by Krishnamurthy is satisfactory for $\frac{v_s}{U_1} = 0, 0{\cdot}005, 0{\cdot}010$ but crossplots show that a further expression should be added for $\frac{v_s}{U_1} = 0{\cdot}002$ or $0{\cdot}003$ so that linear interpolation with respect to $\frac{v_s}{U_1}$ leads to satisfactory values of c_f over the entire range.

(iv) The effects of surface roughness and non-homogenity of suction are not expected to be important in Sarnecki's layers on a nylon surface as the porosity scale is usually less than the predicted sublayer thickness. Measurements on a Vyon surface in zero pressure gradient would remove the present uncertainty, however.

(v) The effects of adverse pressure gradient, overall Reynolds number, and blockage to the suction flow all need careful investigation.

(vi) The behaviour of shear stress distributions indicates that the present inner region assumptions are, as expected, inaccurate near the start of the suction surface and further investigation is needed to understand the behaviour of the turbulent layer in these conditions especially as strip suction may be of some practical importance.

(vii) The inner region analyses of Tennekes and of Stevenson appear to offer no advantages over the present profile assumptions.

(viii) Experiments should be conducted to find the displacement effects for flattened pitots.

The present 'intermittency' model for velocity profiles has been used by McQuaid[11] for injection conditions in the range $0 \leqslant \frac{v_0}{U_1} \leqslant 0{\cdot}008$ with very satisfactory results using the value of mixing length constant (κ) appropriate to his experimental arrangement and found from measured profiles at zero and very large transpiration rates. The factors influencing κ are unknown at present and so on average value must be used to provide profile relationships suitable for a calculation method. The mean value $\kappa = 0{\cdot}419$ used previously in the solid surface family has been retained here.

6. *Acknowledgements.*

The author thanks Drs. M. R. Head and J. McQuaid for helpful discussions during the course of this investigation. Thanks are due also to Miss Susan Grey and Mrs. M. Rowe who assisted with the numerical work. The kindness of Drs. A. J. Sarnecki, M. Coantic, and H. Tennekes who supplied details of their suction measurements is also greatly appreciated.

LIST OF SYMBOLS

c_f	Local skin-friction coefficient
d	Constant of integration in bilog law
H	Profile shape factor $\left(= \frac{\delta^*}{\theta} \right)$
R_θ, R_{δ_s}	Reynolds numbers, $R_\theta = \frac{U_1 \theta}{\nu}$; $R_{\delta_s} = \frac{U_1 \delta_s}{\nu}$
U_1	Local freestream velocity
u	Local x-component of overall mean velocity in the boundary layer
u_t	Corresponding component of velocity within the 'turbulent fluid' taken as a mean over 'time turbulent'
U_τ	Wall friction velocity
$\frac{U_1}{\nu}$	Unit Reynolds number
v, w	Refer to fully turbulent and viscous sublayer regions of the u_t velocity distribution
v_0	Transpiration velocity (positive for injection)
$v_s (= -v_0)$	Suction velocity
x	Distance measured downstream from the start of suction
y	Distance measured normal to wall
y_a	Height of intersection between (extrapolated) sublayer and fully-turbulent inner-region velocity profiles.
α	Damping coefficient appearing in van Driest's blending region analysis
α_0	Value of α for zero transpiration
γ_s	'Intermittency' factor used in profile model
δ_1, δ_s	Boundary-layer thicknesses
δ^*	Displacement thickness
Δ, Δ_i	Inner region pressure-gradient parameters defined in Section 4.5
θ	Momentum-loss thickness
κ	Mixing-length constant
λ	Bilog. law parameter
ν	Kinematic viscosity
ρ	Density of fluid
τ	Shear stress
τ_0	Wall shear stress

REFERENCES

No.	Author(s)	Title, etc.
1	T. J. Black and A. J. Sarnecki ..	The turbulent boundary layer with suction or injection. A.R.C. R. & M. 3387 (1958)
2	D. Coles	The law of the wake in the turbulent boundary layer. *J. Fluid Mech*, Vol. 1, pp 191–226. 1956.
3	E. R. van Driest	On turbulent flow near a wall. *J. Aeronaut. Sci.*, Vol. 23, pp 1007–1011 and 1036. (1956).
4	R. A. Dutton	The effects of distributed suction on the development of turbulent boundary layers. A.R.C. R. & M. 3155. (1958).
5	A. Favre, R. Dumas and E. Verollet ..	Couche limite sur paroi plane poreuse avec aspiration. *Pub. Sci. et Tech. du Min. de l'Air*, No. 377. (1961).
6	A. Favre, R. Dumas, E. Verollet and M. Coantic	Couche limite sur paroi plane poreuse avec aspiration; presented at the AGARD Specialists meeting *Recent developments in Boundary Layer Research*, May 1965, Naples.
7	M. R. Head	Approximate calculations of the laminar boundary layer with suction, with particular reference to the suction requirements for boundary-layer stability on aerofoils of different thickness chord ratios. A.R.C. R. & M. 3124. (1957).
8	J. M. Kay	Boundary-layer flow along a flat plate with uniform suction. A.R.C. R. & M. 2628. (1948).
9	R. Krishnamurthy	Private communication. (1964).
10	J. McQuaid	Experiments on incompressible turbulent boundary layers with distributed injection. A.R.C. R. & M. 3549. (1967).
11	J. McQuaid	The calculation of turbulent boundary layers with injection. A.R.C. R. & M. 3542. (1967).
12	J. McQuaid	Ph. D. Dissertation, Cambridge University. (1966).
13	V. C. Patel	Ph.D. Dissertation, Cambridge University. (1965).
14	A. J. Sarnecki	Ph.D. Dissertation, Cambridge University. (1959).
15	T. N. Stevenson	A law of the wall for turbulent boundary layers with injection. Coll. Aero. Cranfield, Rep. Aero. no. 166. (1963).

No.	*Author(s)*	*Title, etc.*
16	H. Tennekes	.. Similarity laws for turbulent boundary layers with suction or injection. *J. Fluid Mech.*, Vol. 21, Pt. 4, pp 681–703. 1964.
17	B. G. J. Thompson ..	.. The calculation of shape-factor development in incompressible turbulent boundary layers with or without transpiration. AGARDograph 97. (1965).
18	B. G. J. Thompson ..	.. A new two-parameter family of mean velocity profiles for incompressible turbulent boundary layers on smooth walls. A.R.C. R. & M. 3463. (1965).
19	B. G. J. Thompson ..	.. An experimental investigation into the behaviour of the turbulent boundary layer with distributed suction in regions of adverse pressure gradient. A.R.C. R. & M. 3621 (1969).

APPENDIX

The Analytic Approximation to the New Skin-Friction Law (*Krishnamurthy* (1964)).

The three expressions are of the general form,

$$\log_e c_f = AH + B, \text{ where } A, B \text{ are } f(R_\theta)$$

Putting $z = \log_e R_\theta$, we have,

$$\text{for } \frac{v_s}{U_1} = 0,\ A = 0{\cdot}019521 - z(0{\cdot}386768 - z(0{\cdot}028345 - 0{\cdot}0007017\, z)),$$

$$B = 0{\cdot}191511 - z(0{\cdot}834891 - z(0{\cdot}062588 - 0{\cdot}001953\, z)),$$

$$\text{for } \frac{v_s}{U_1} = 0{\cdot}005,\ A = 1{\cdot}07085 - z(0{\cdot}831747 - z(0{\cdot}106843 - 0{\cdot}004428\, z)),$$

$$B = z(0{\cdot}015834 - z(0{\cdot}047968 - 0{\cdot}003308\, z)) - 2{\cdot}338049,$$

$$\text{and finally for } \frac{v_s}{U_1} = 0{\cdot}010,$$

$$A = -1{\cdot}00747 - \exp(10{\cdot}97531 - 8{\cdot}1080555 \log_e z),$$

$$B = 110{\cdot}92 \exp(-1{\cdot}06\, z) - 2{\cdot}94.$$

TABLE 1

Permissible Roughness Height for Sarnecki[14] *Layers.*
(Skin-Friction Values from Momentum Equation).

$$\frac{U_1}{\nu} = 32500 \text{ per inch}$$

Profile	c_f	$\frac{v_0}{U_1}$	$\frac{v_0}{U_\tau}$	$\frac{U_\tau y_a}{\nu}$	y_a ins.
10N098	0·0049	−0·00098	−0·0198	12·4	0·0077
30N098	0·0048	−0·00098	−0·020	12·4	0·0078
50N098	0·0033	−0·00098	−0·024	13·0	0·0098
30N246	0·0062	−0·00246	−0·044	17·0	0·0094
40N246	0·0060	−0·00246	−0·045	17·5	0·0098
30N374	0·0082	−0·00374	−0·058	25·0	0·012
40N374	0·0068	−0·00374	−0·064	32·2	0·016
50N374	0·0075	−0·00374	−0·061	27·5	0·0137
10N443	0·0087	−0·00443	−0·067	40·5	0·0182
30N443	0·0084	−0·00443	−0·068	45·5	0·0216
50N443	0·0088	−0·00443	−0·067	38·5	0·0178

TABLE 2

Functions used in Computing Velocity Profile Shapes, and the Skin-Friction Law.

$\frac{v_s}{U_\tau}$	λ	$\frac{U_\tau y_a}{\nu}$	$\log_{10}\frac{U_\tau d}{\nu}$
0·0010	0·997	11·2068	362·6
0·0050	0·986	11·3701	73·1
0·0100	0·973	11·5836	35·37
0·0200	0·943	12·4800	17·16
0·0300	0·907	13·8119	11·0
0·0400	0·860	15·8855	7·81
0·0450	0·828	17·5362	6·68
0·0500	0·792	19·4709	5·76
0·0600	0·690	26·1834	4·19
0·0650	0·605	34·0143	3·382
0·0675	0·550	41·0282	2·96
0·0700	0·480	55·3058	2·495
0·0701	0·477	56·3132	
0·0702	0·473	57·3718	
0·0703	0·470	58·4877	
0·0704	0·466	59·6681	
0·0705	0·463	60·9215	
0·0706	0·460	62·2587	
0·0707	0·456	63·6928	
0·0708	0·453	65·2406	
0·0709	0·449	66·9240	
0·0710	0·446	68·7722	2·286
0·0711	0·443	70·8258	
0·0712	0·439	73·1438	
0·0713	0·436	75·8176	
0·0714	0·432	79·0024	
0·0715	0·429	83·0017	
0·0716	0·426	88·5925	
0·0717	0·422	100·9141	2·14

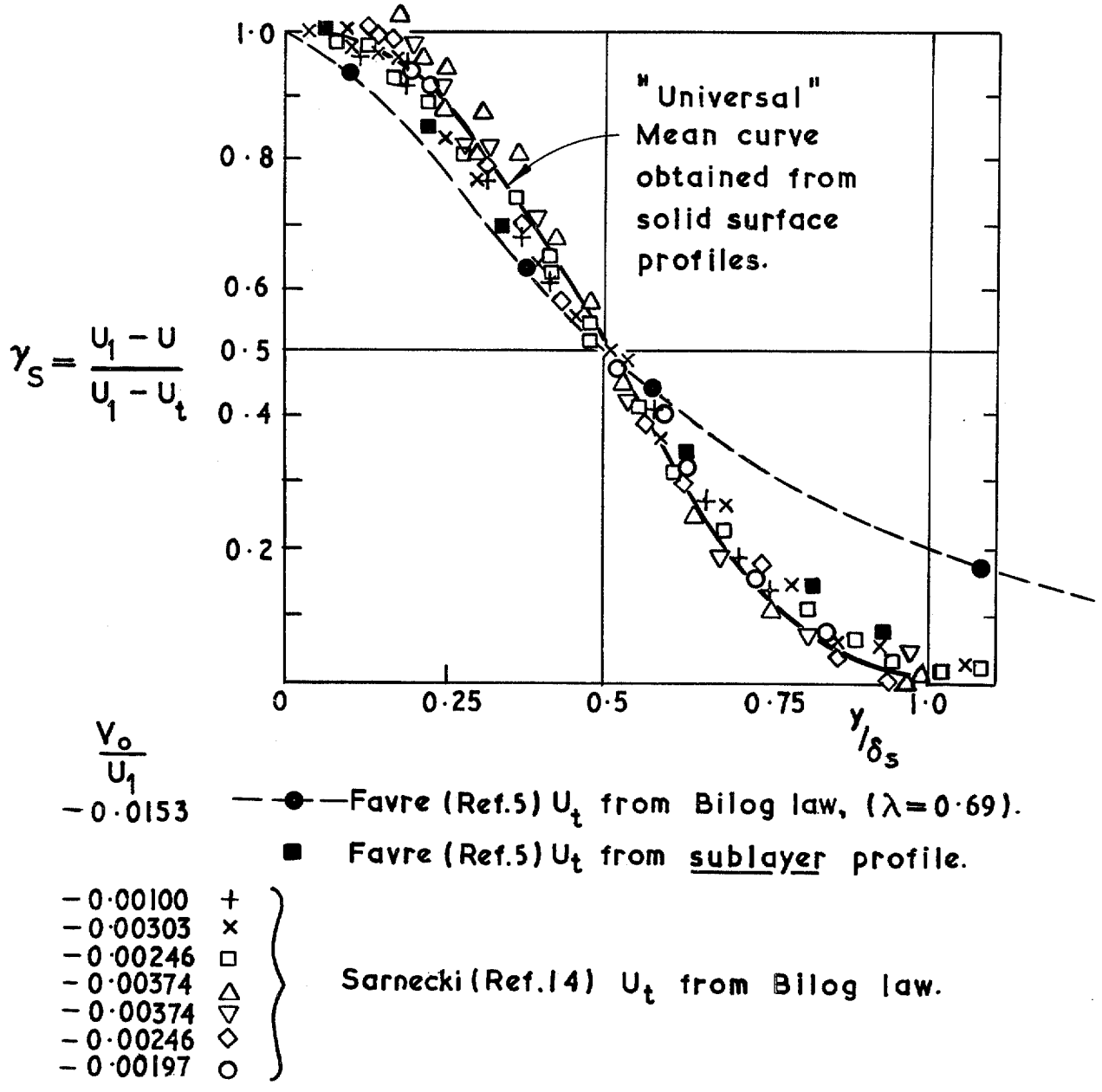

FIG. 1. Intermittency hypothesis applied to suction profiles.

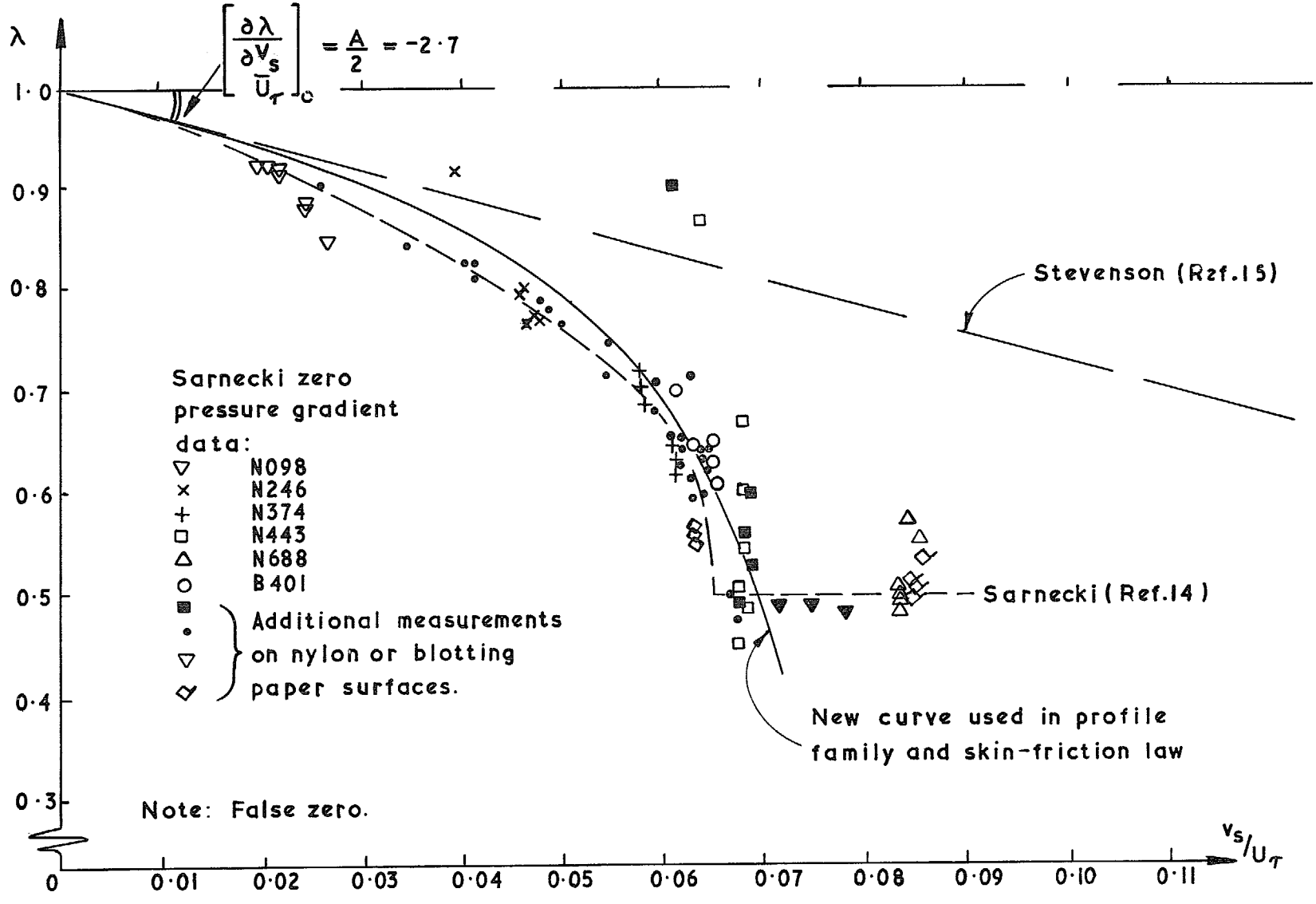

FIG. 2. Correlation of zero pressure gradient Bilog. profile parameter λ.

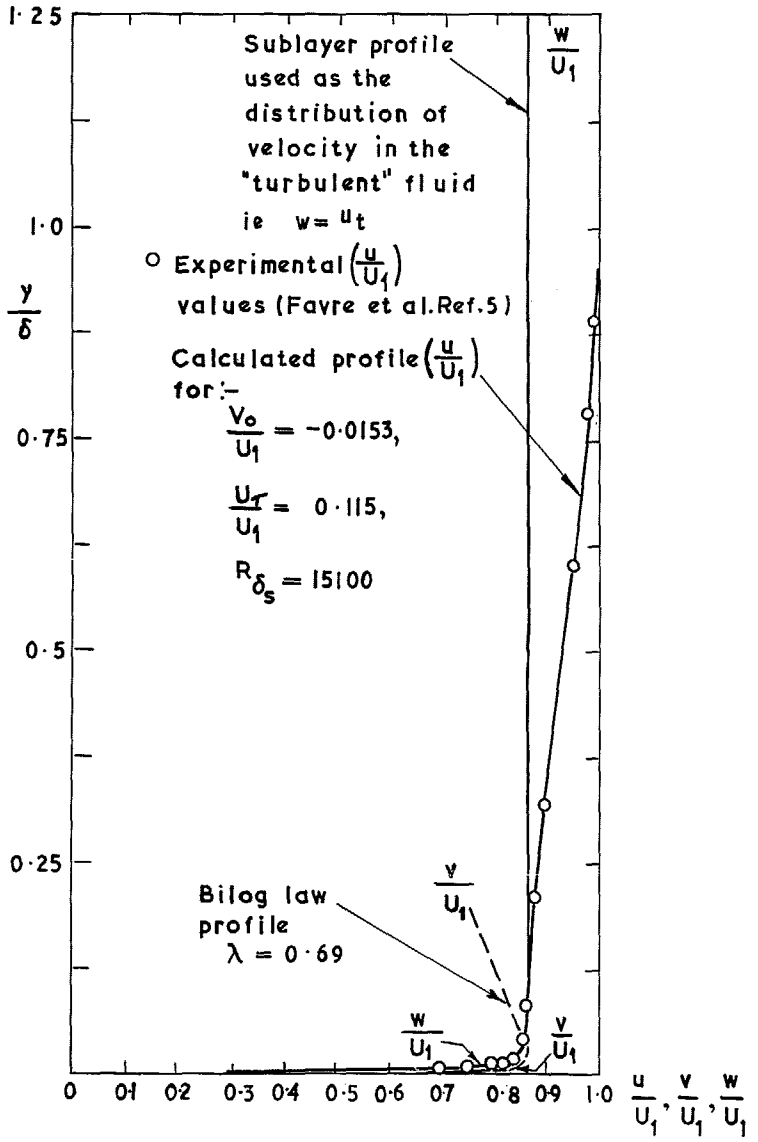

FIG. 3. Comparison of a calculated suction profile with experiment.

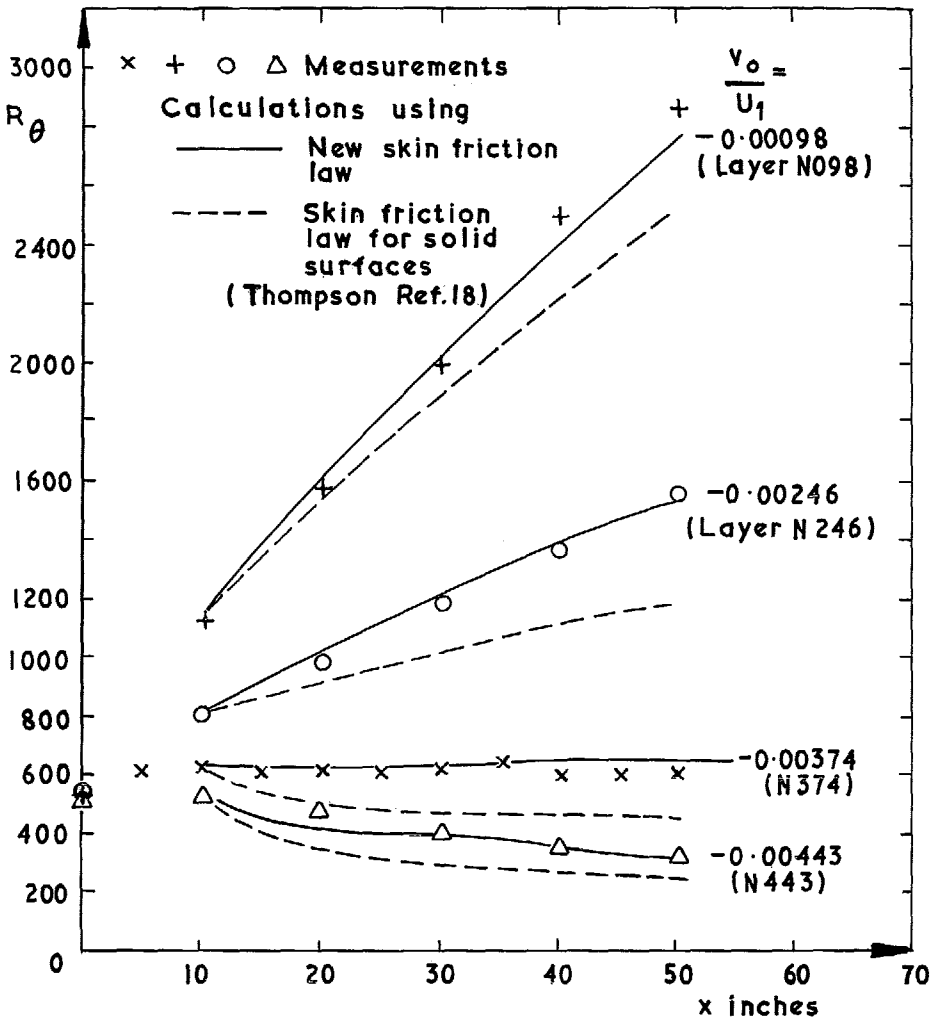

FIG. 4. Comparison of calculated momentum developments with Sarnecki's zero pressure gradient measurements on a nylon suction surface.

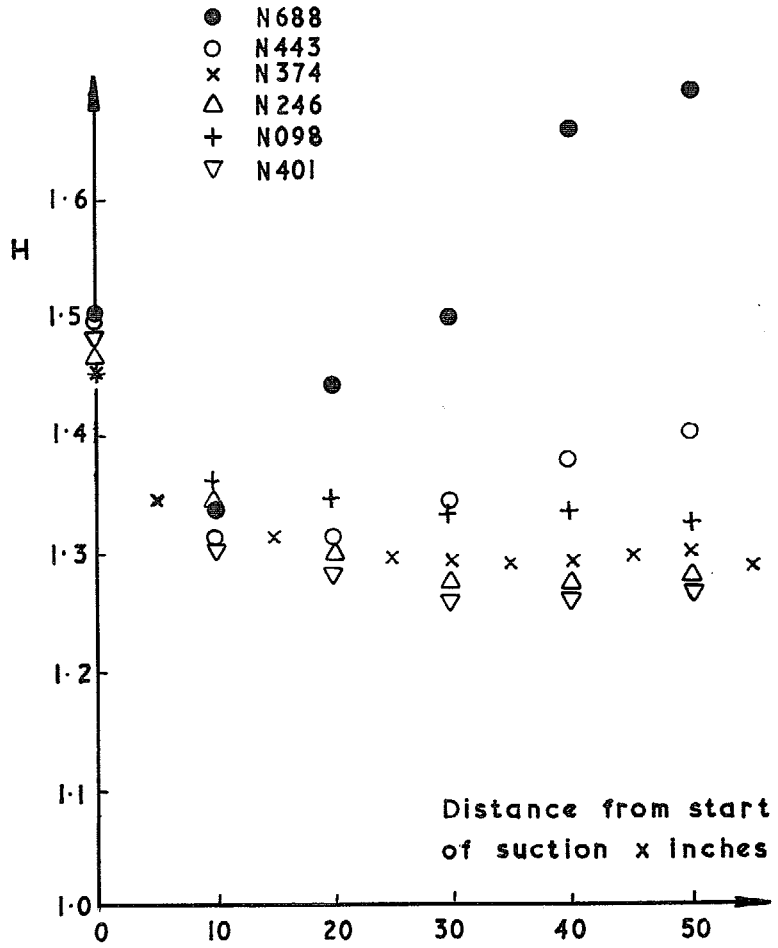

FIG. 5. Shape factor growth in layers with suction. Sarnecki[14].

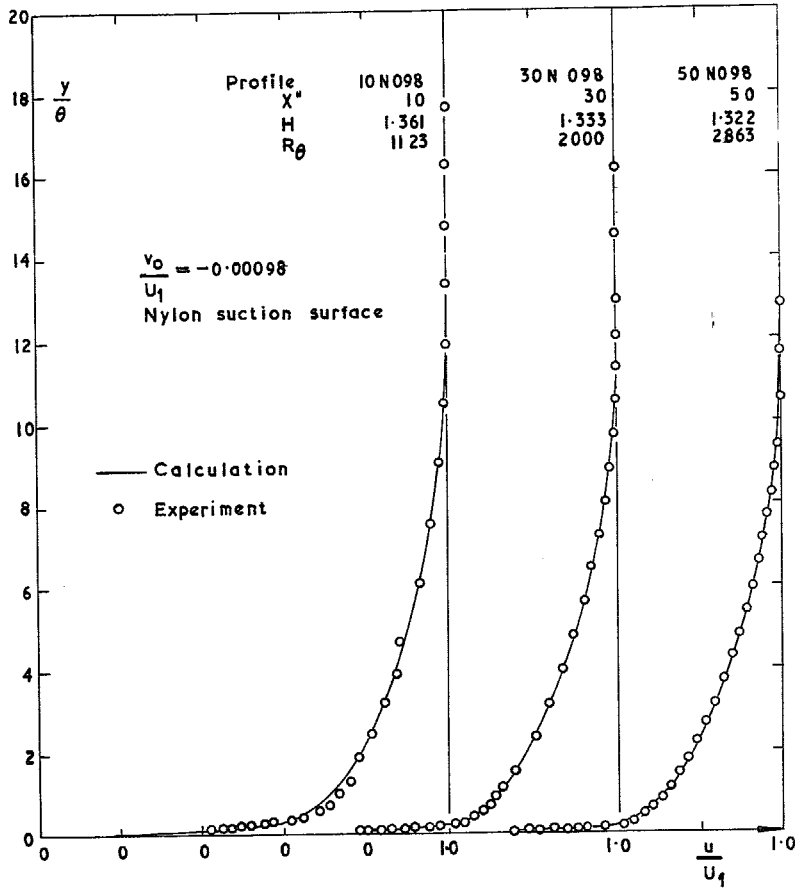

FIG. 6. Profile comparisons. Sarnecki N098.

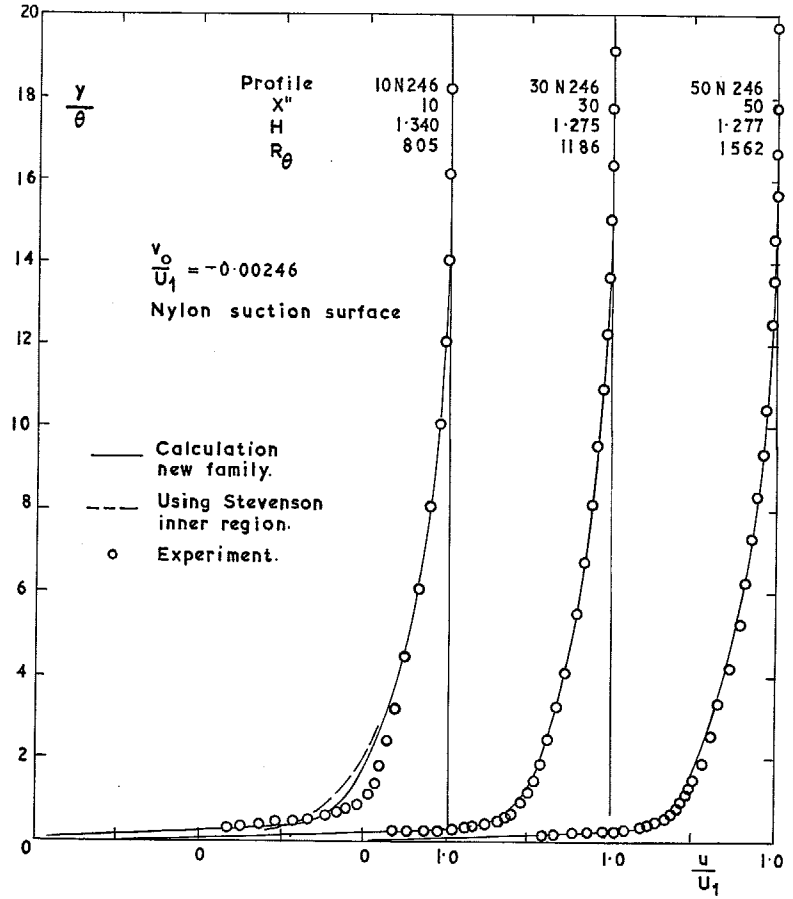

FIG. 7. Profile comparisons. Sarnecki layer N246.

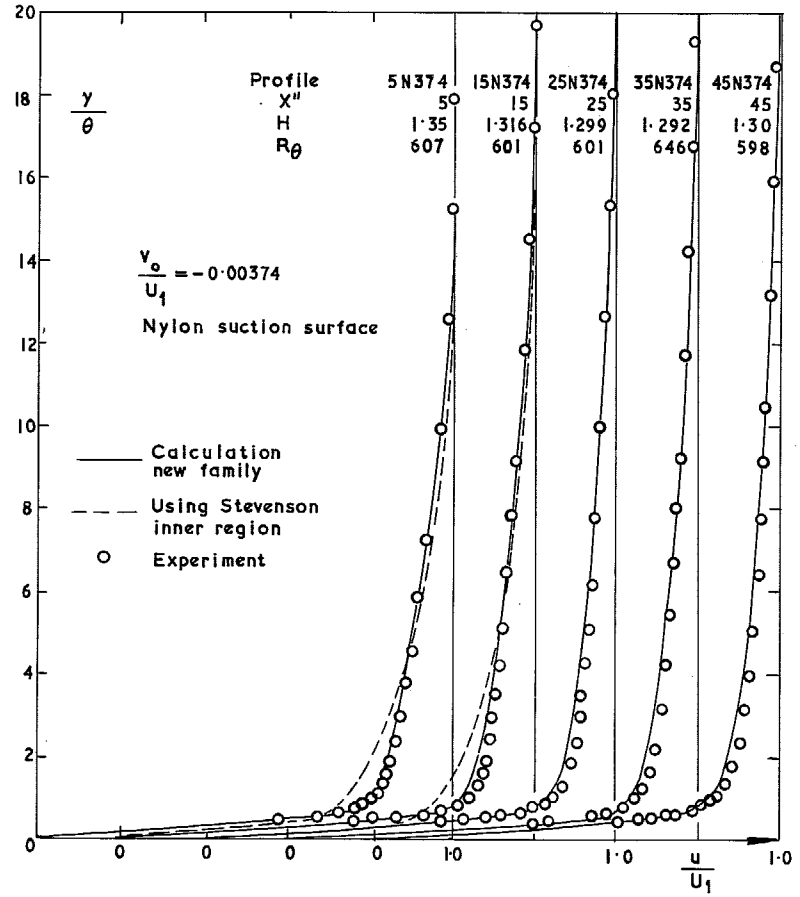

FIG. 8. Profile comparisons. Sarnecki layer N374.

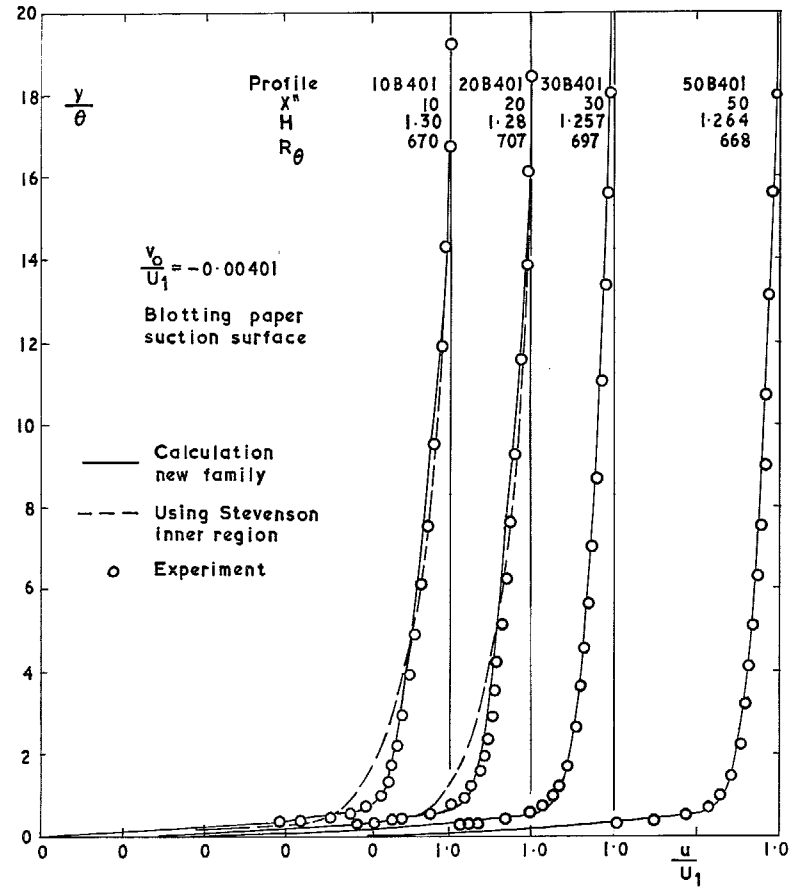

FIG. 9. Profile comparisons. Sarnecki layer B401.

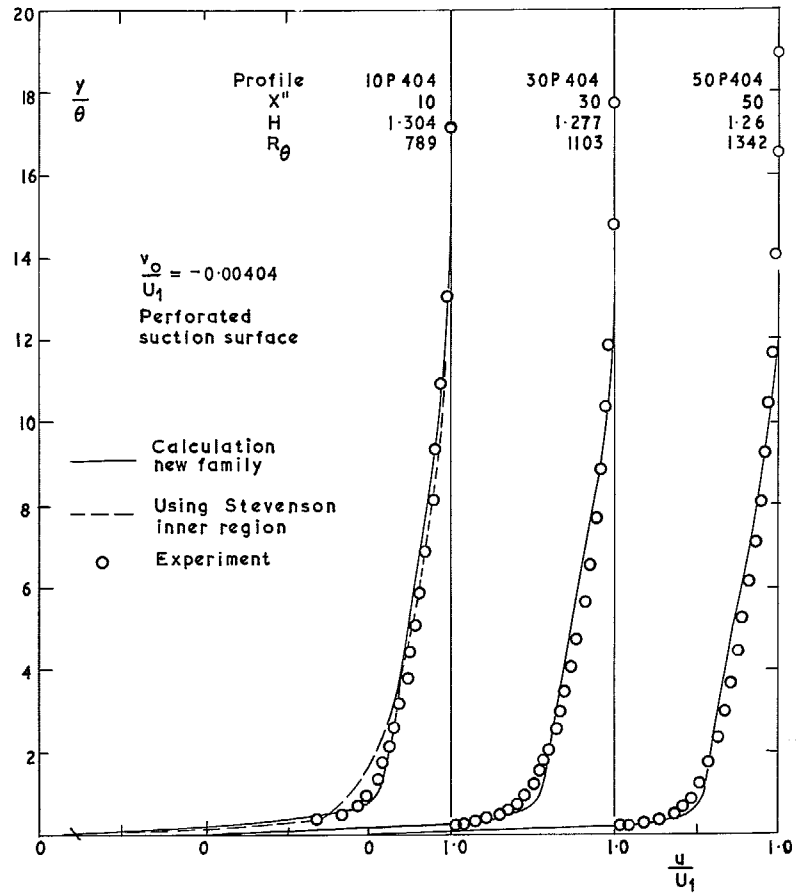

FIG. 10. Profile comparisons. Sarnecki layer P404.

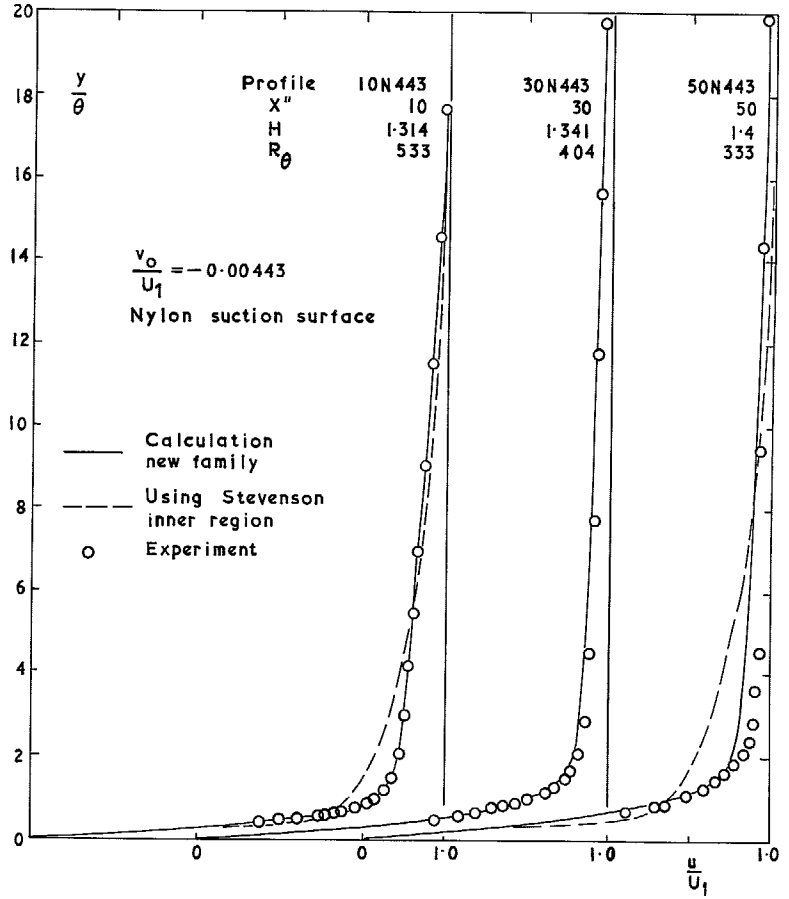

FIG. 11. Profile comparisons. Sarnecki layer N443.

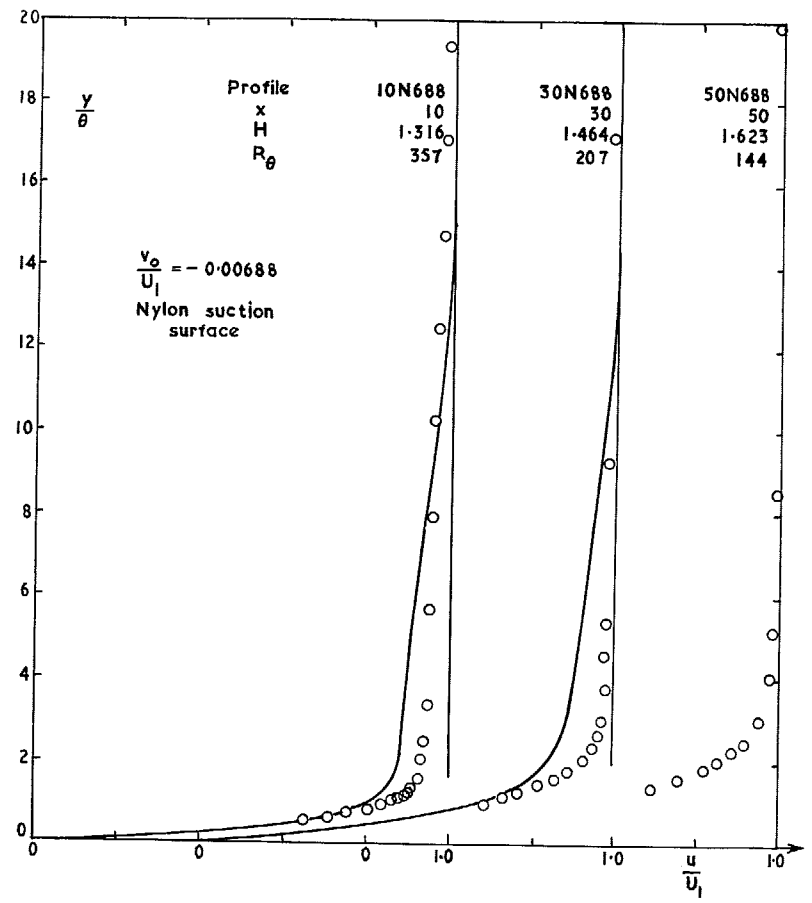

FIG. 12. Profile comparisons. Sarnecki layer N688.

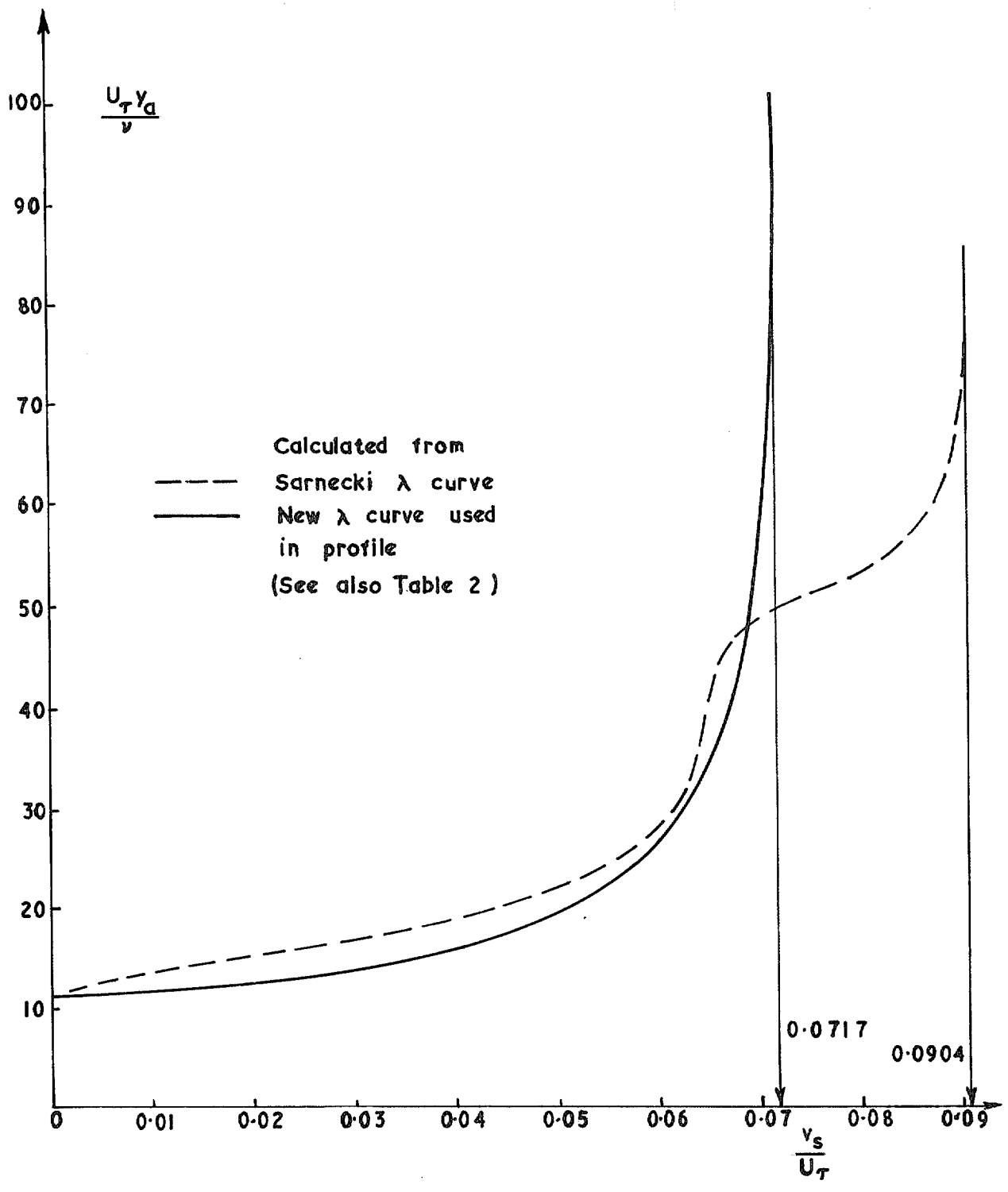

FIG. 13. Variation of Reynolds number based upon intersection between sublayer and Bilog. Law.

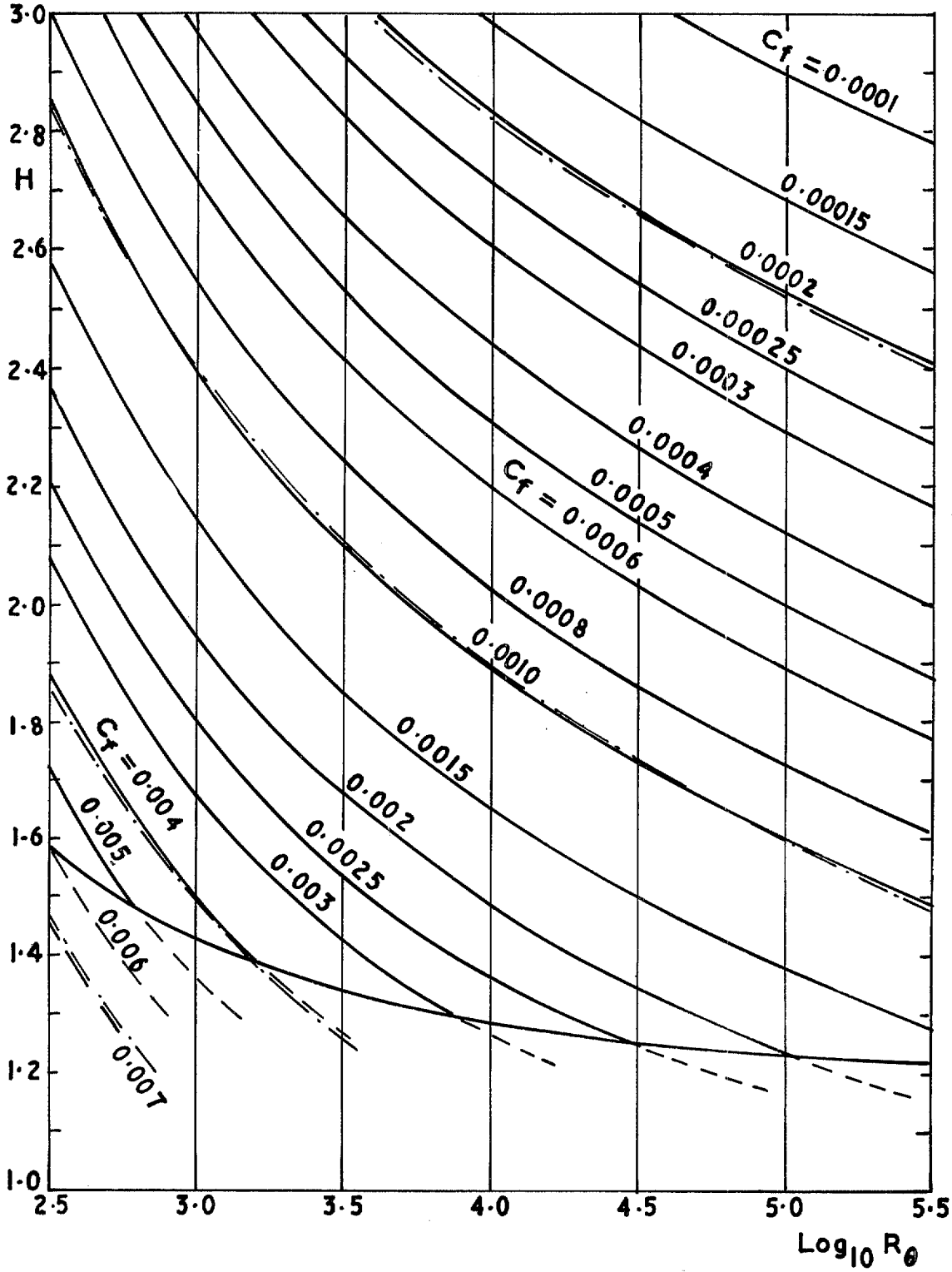

FIG. 14. Skin friction chart for $\frac{v_s}{U_1} = 0{\cdot}000$.

(Analytic approx. shown —·—·—)

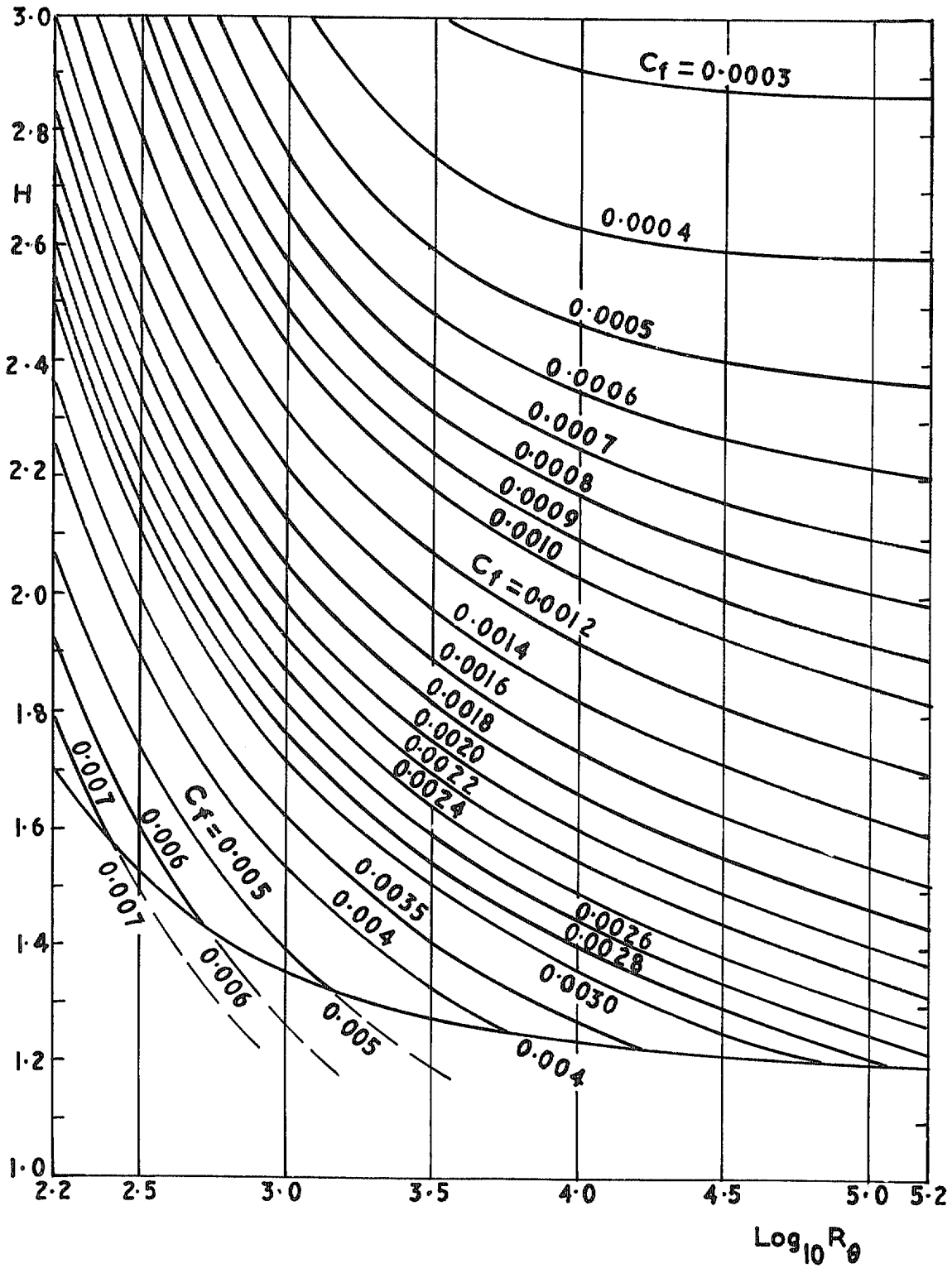

FIG. 15. Skin friction chart for $\frac{v_s}{U_1} = 0{\cdot}001$.

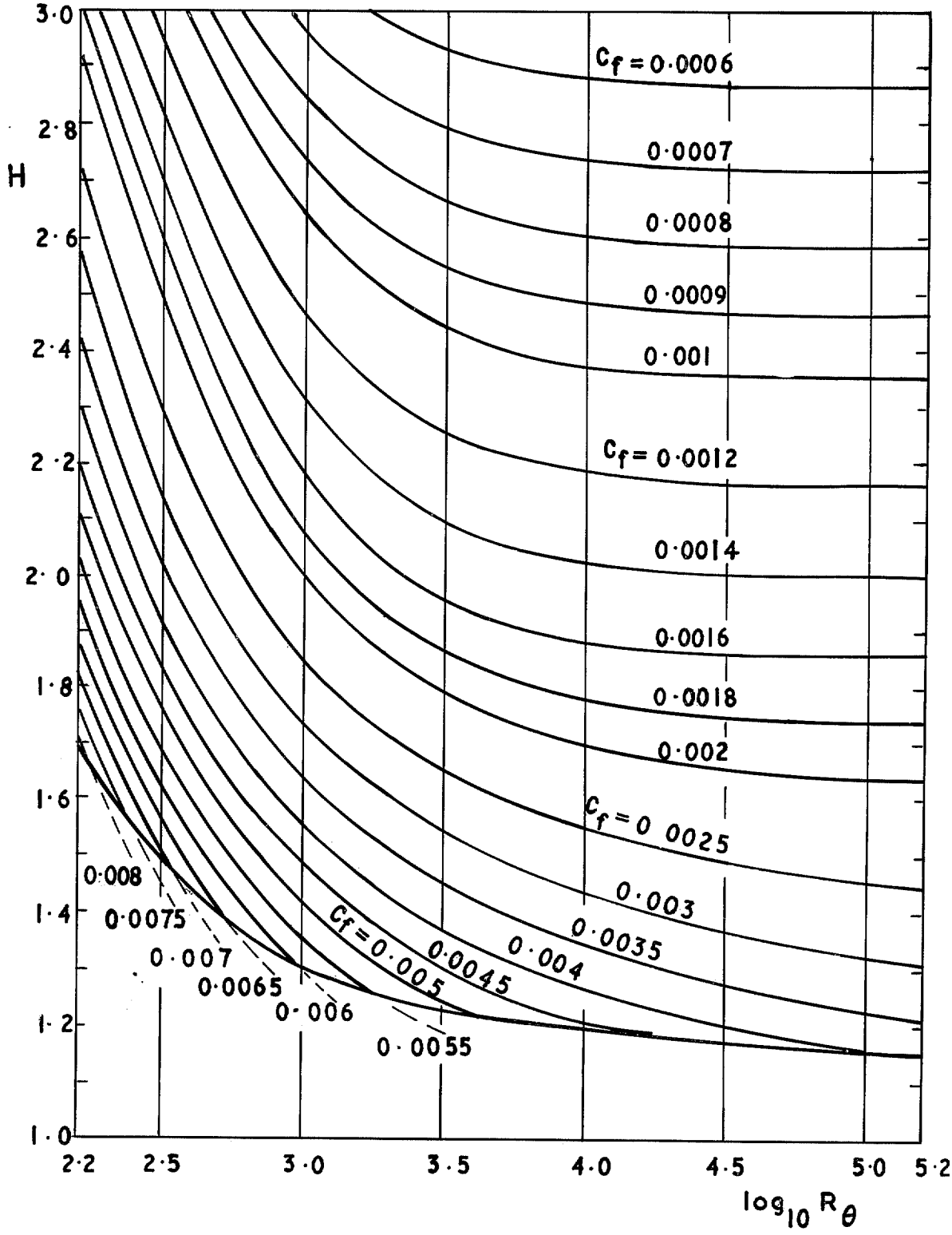

FIG. 16. Skin friction chart for $\frac{v_s}{U_1} = 0·002$.

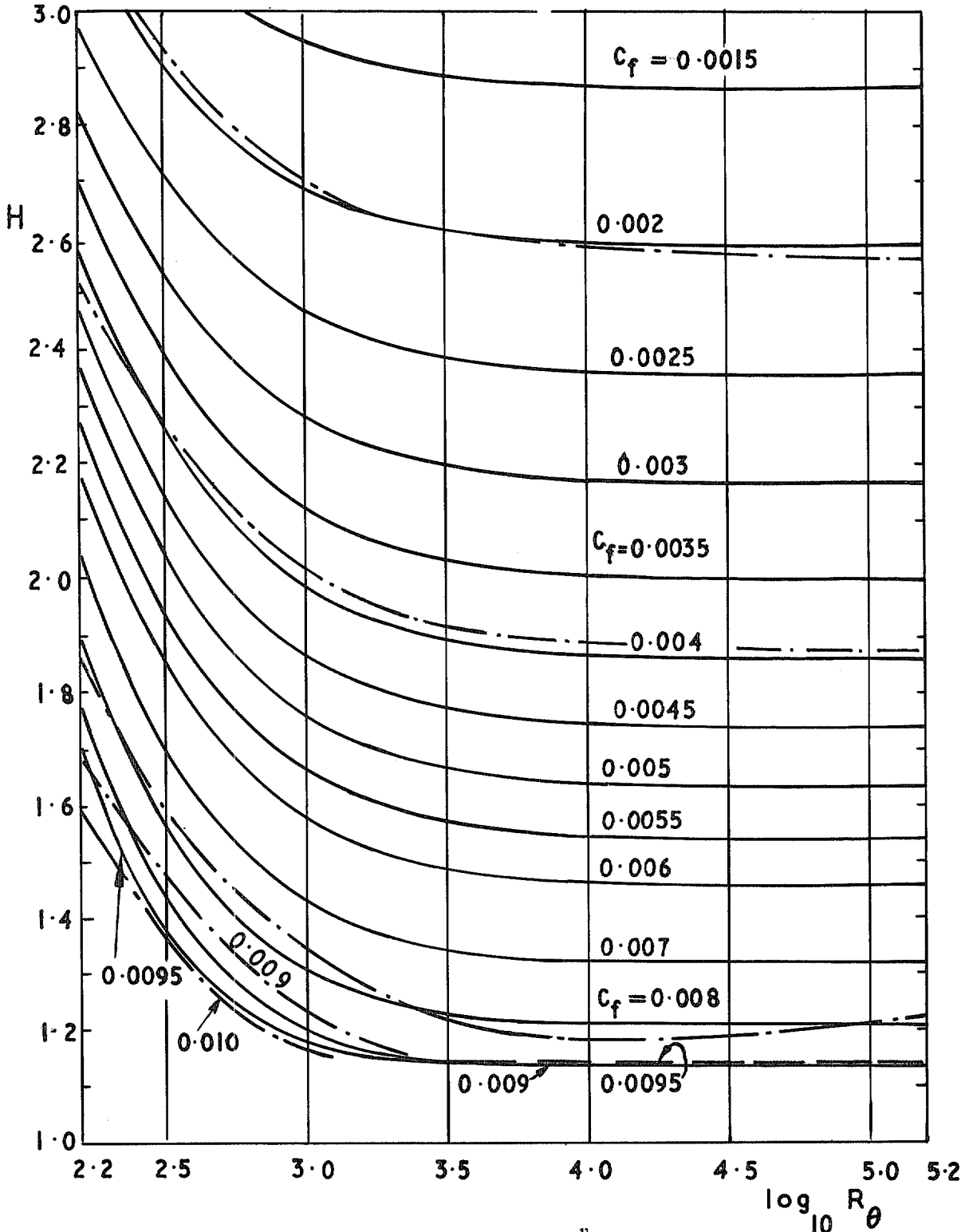

FIG. 17. Skin friction chart $\frac{v_s}{U_1} = 0{\cdot}005$.

(Analytic approx. shown —·—·—)

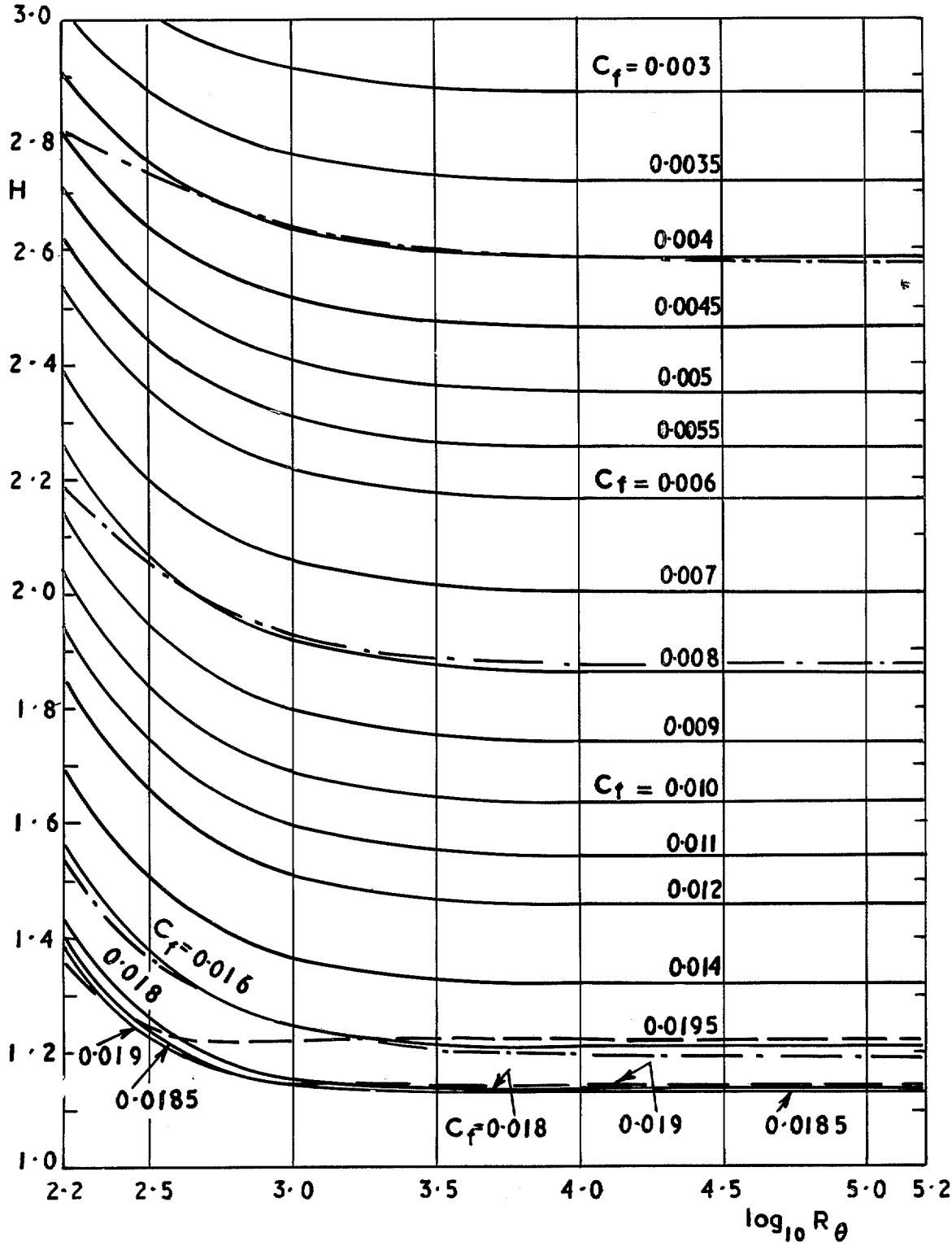

FIG. 18. Skin friction chart for $\frac{v_s}{U_1} = 0{\cdot}010$.

(Analytic approx. shown —·—·—)

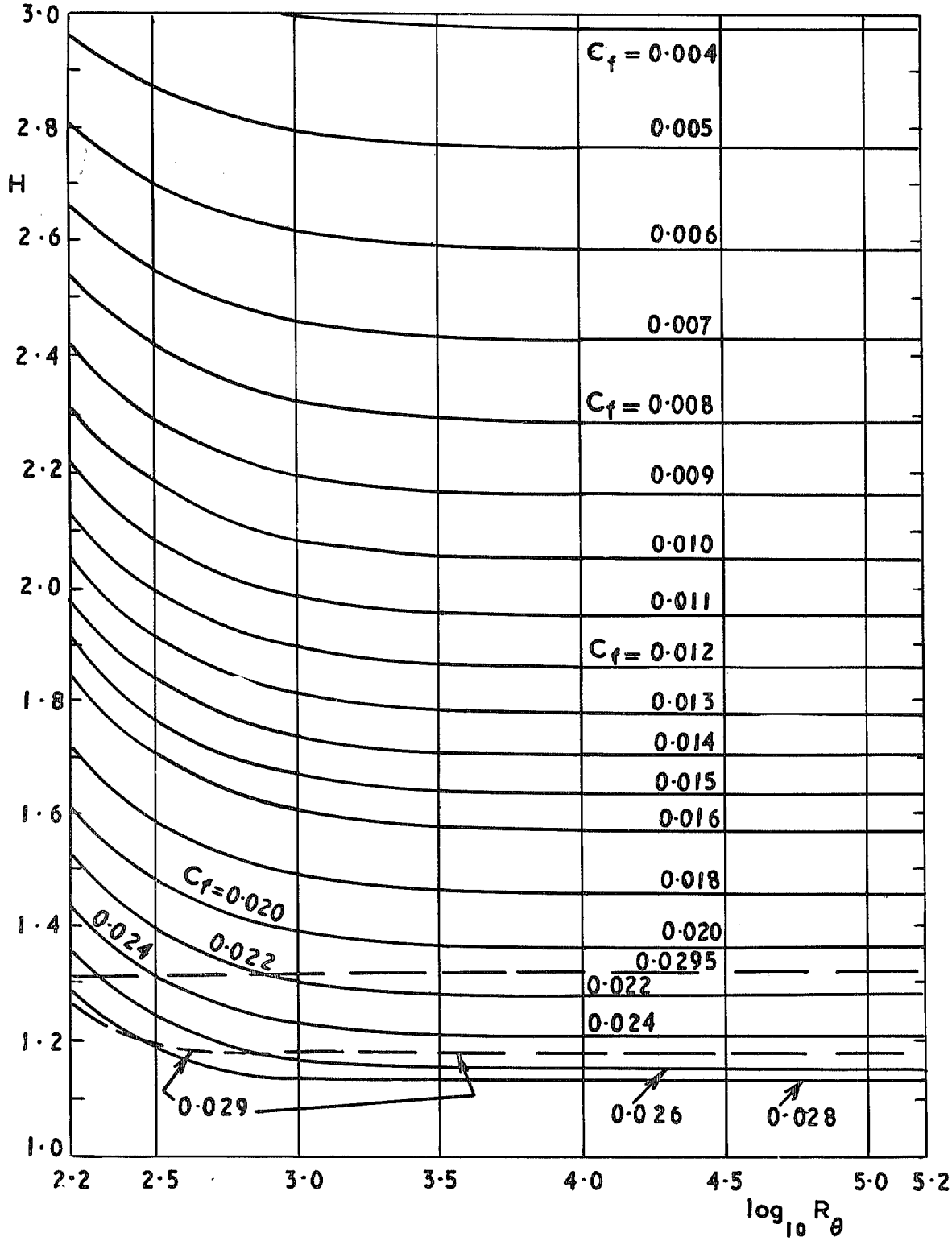

FIG. 19. Skin-friction chart for $\frac{v_s}{U_1} = 0{\cdot}015$.

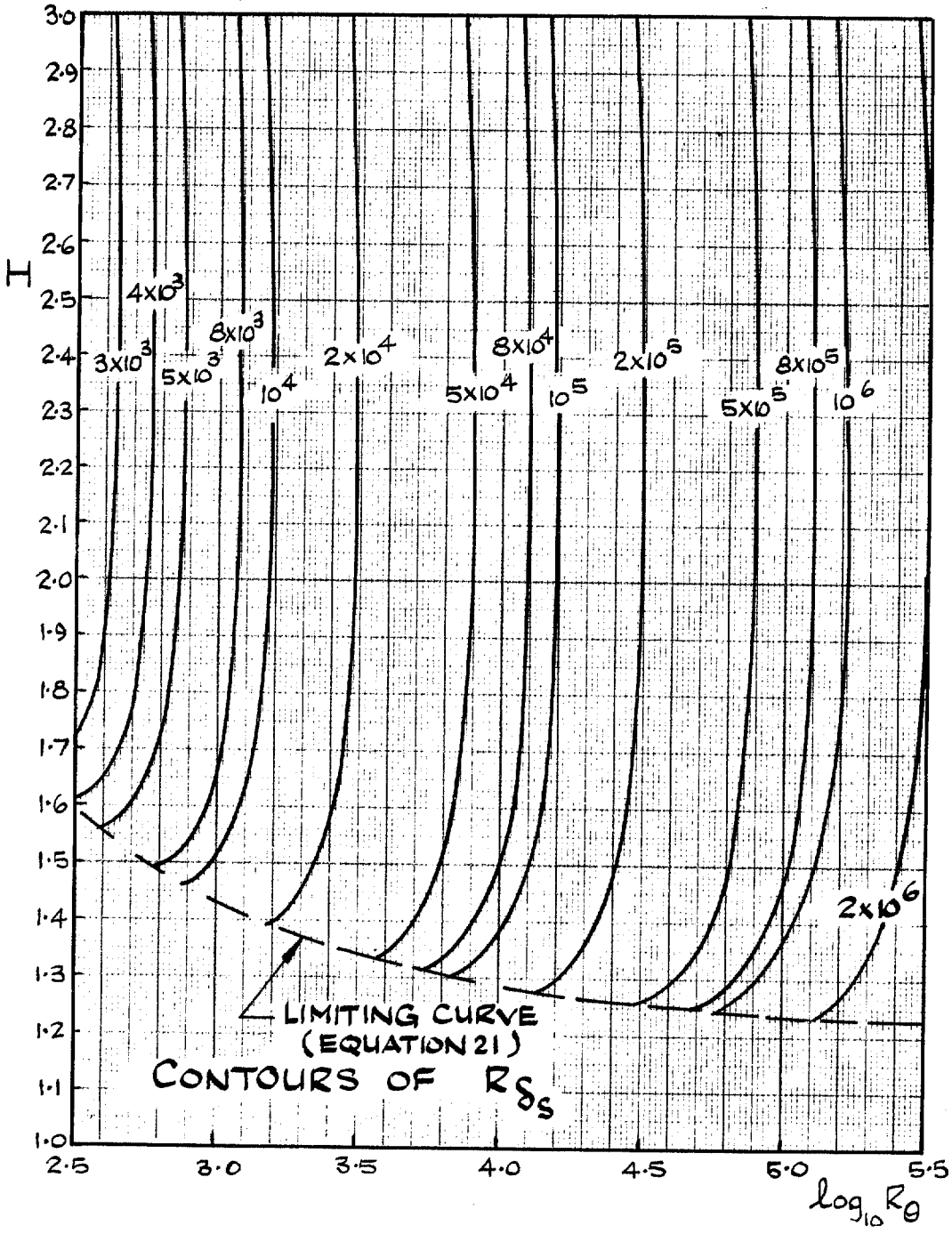

FIG. 20. The relationship between H, R_θ and the profile parameter R_{δ_s} for $\frac{v_s}{U_1} = 0$.

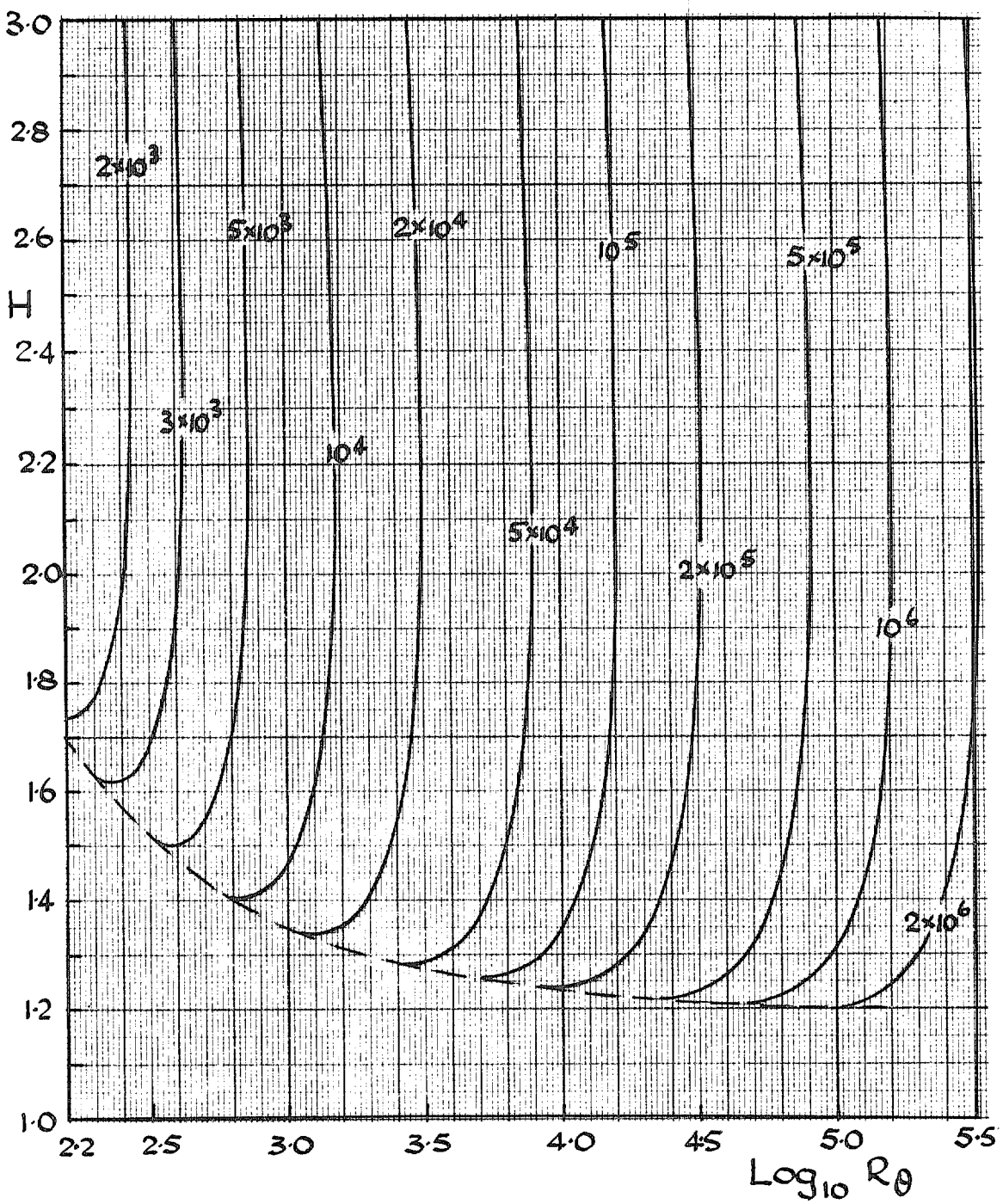

FIG. 21. Variation of R_{δ_s} for $\frac{v_s}{U_1} = 0{\cdot}001$.

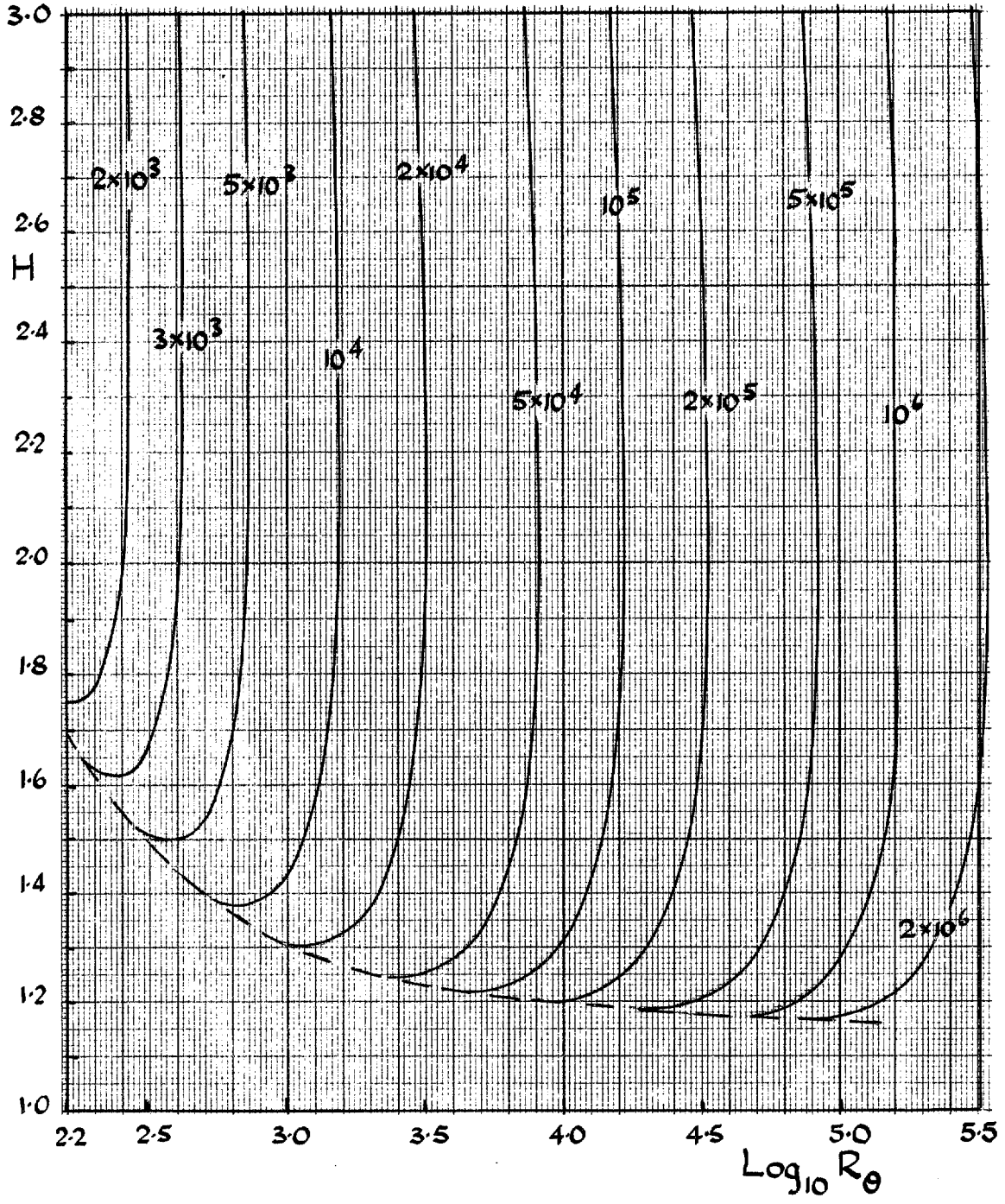

FIG. 22. Variation of R_{δ_s} for $\frac{v_s}{U_1} = 0{\cdot}002$.

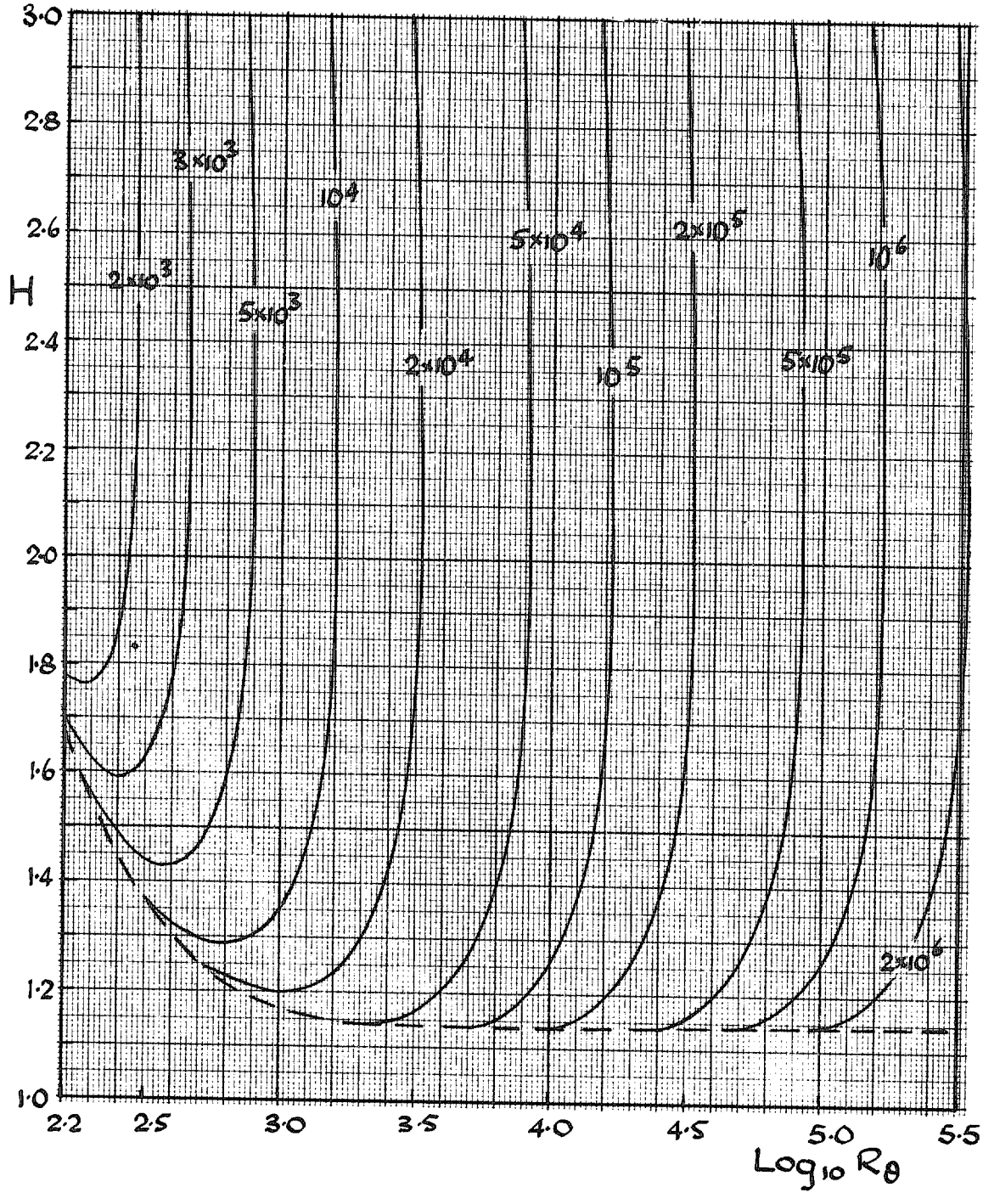

FIG. 23. Variation of R_{δ_s} for $\frac{v_s}{U_1} = 0{\cdot}005$.

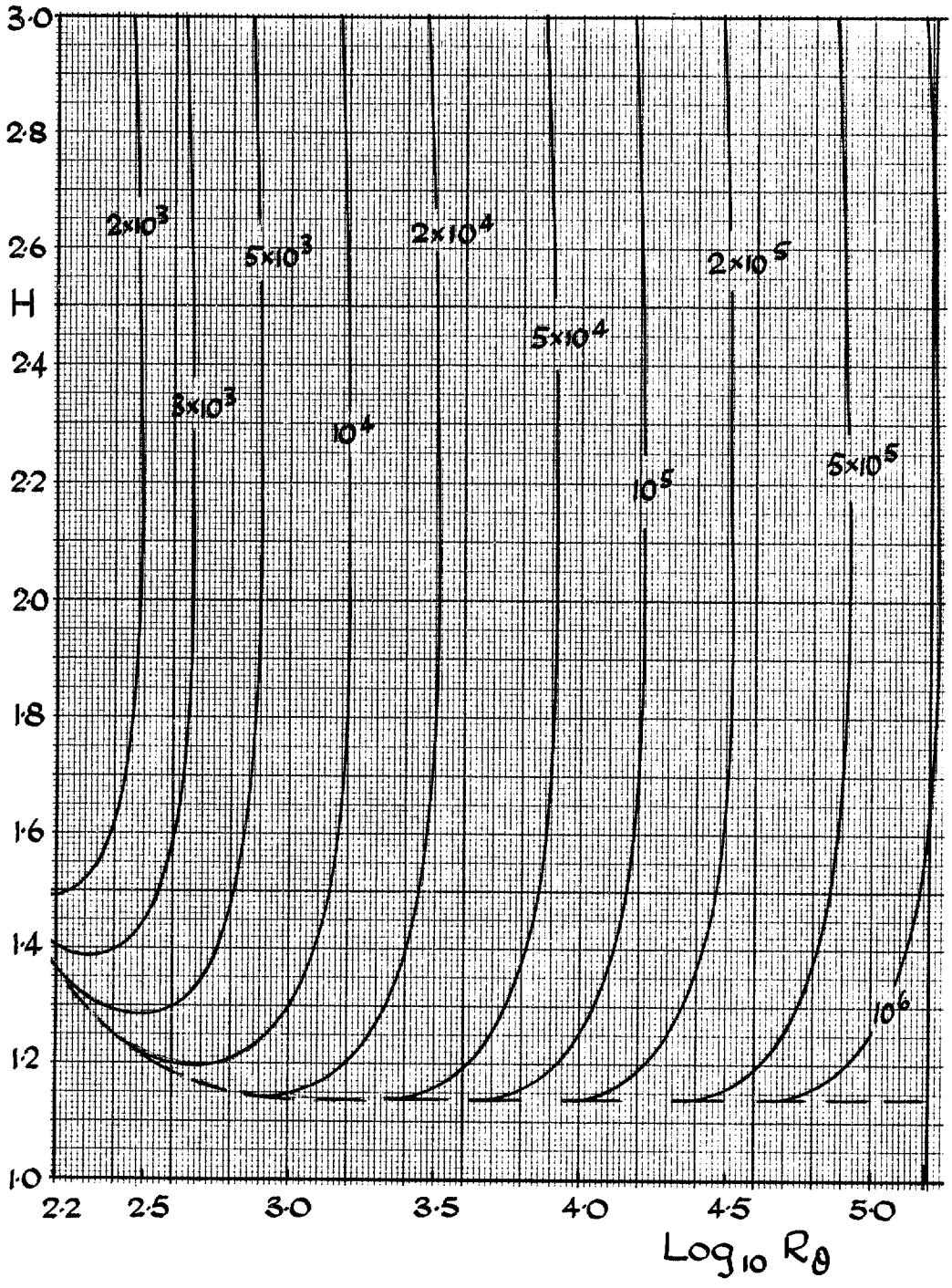

FIG. 24. Variation of R_{δ_s} for $\frac{v_s}{U_1} = 0{\cdot}010$.

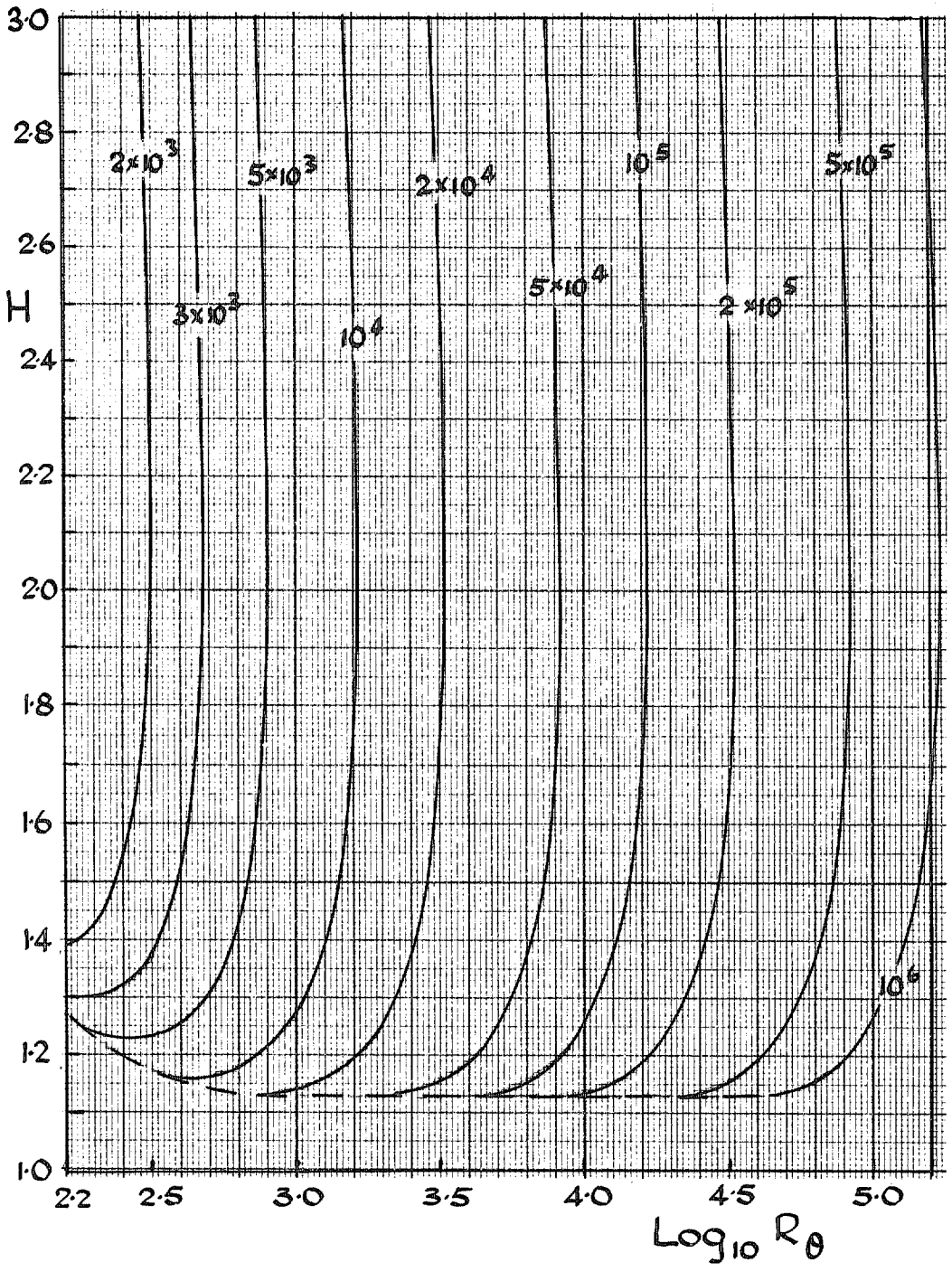

FIG. 25. Variation of R_{δ_s} for $\frac{v_s}{U_1} = 0{\cdot}015$.

31145
FIG. 26

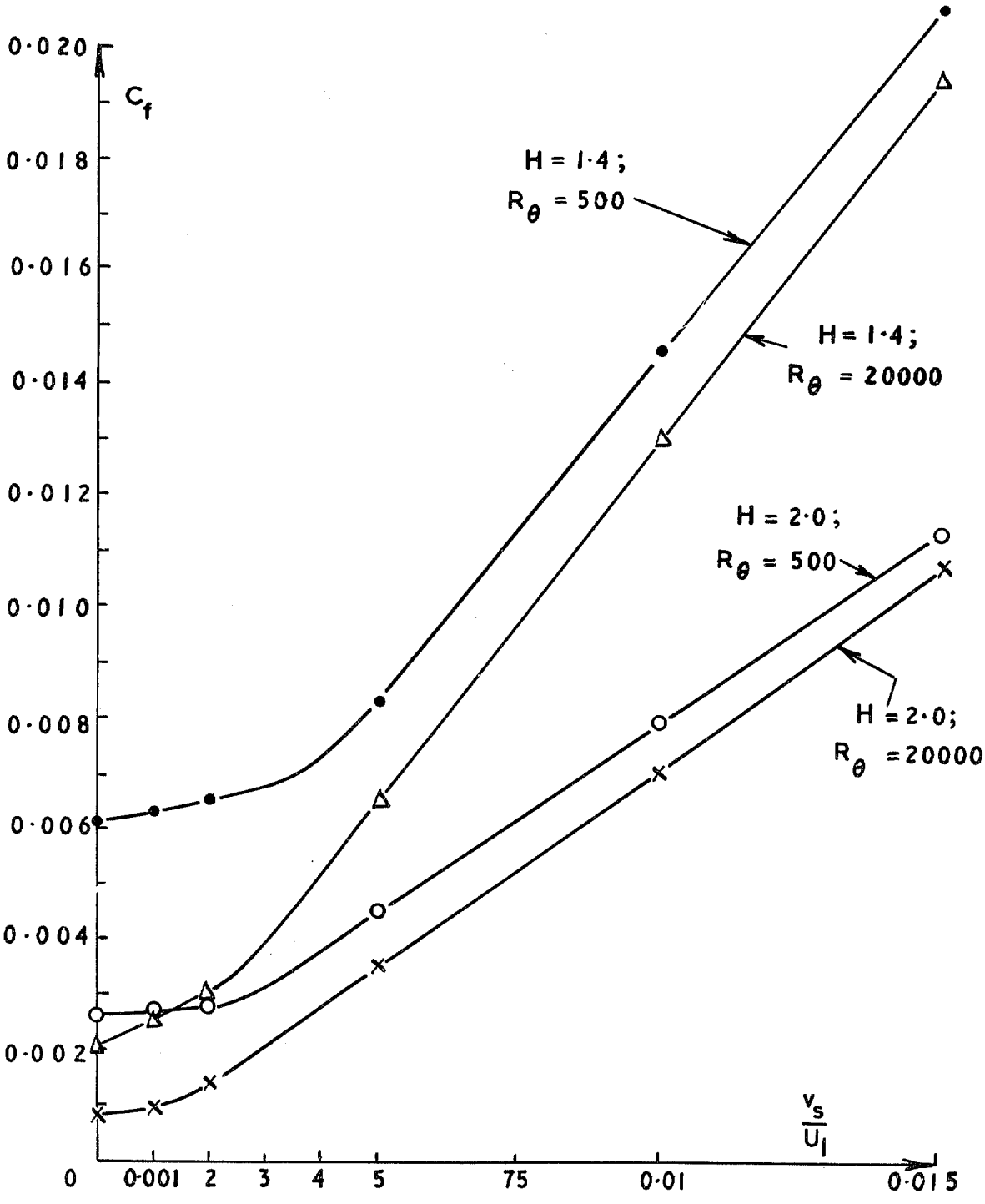

FIG. 26. Typical variation of skin friction coefficient with suction rate (from Figs. 14 to 19).

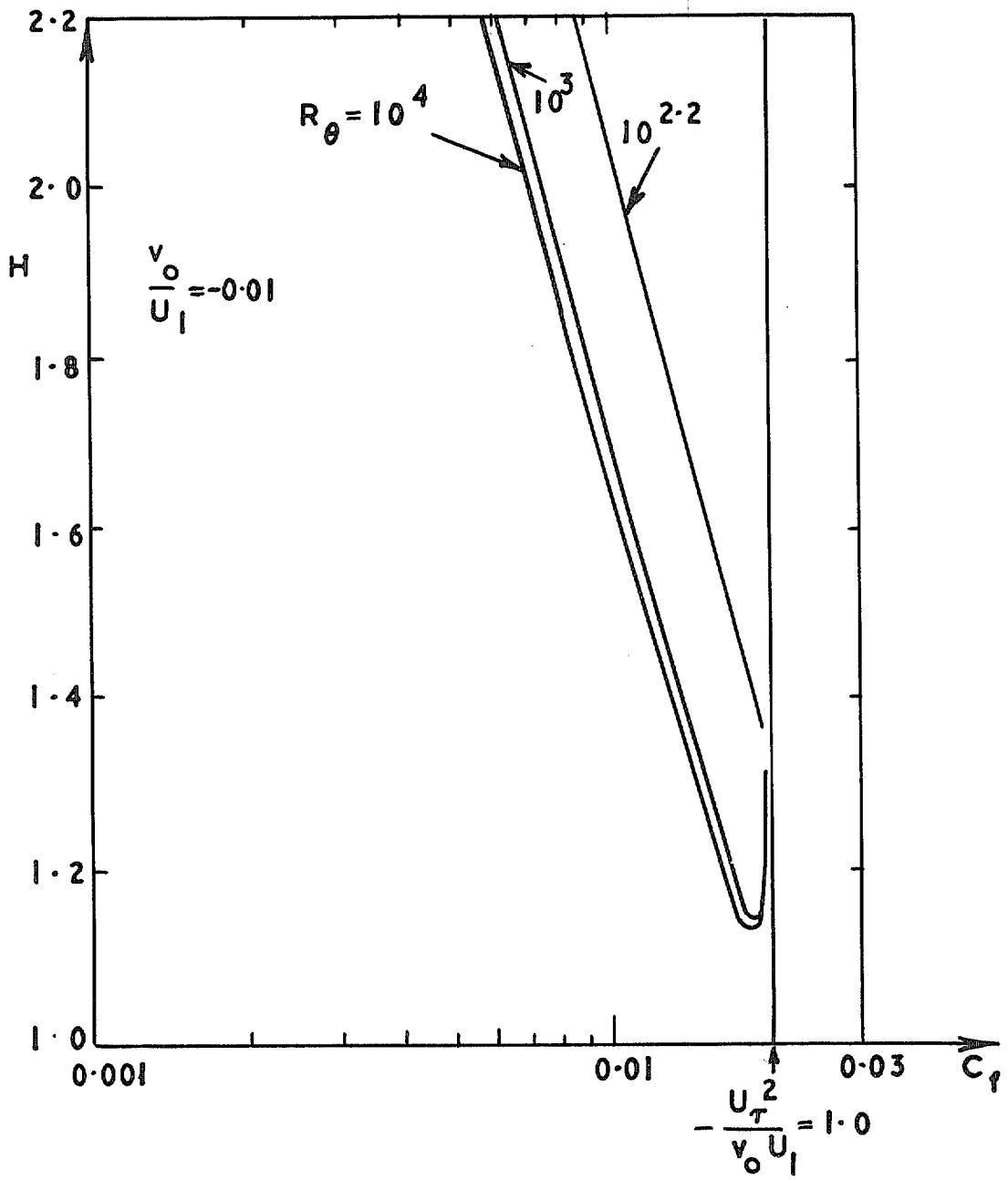

FIG. 27. Double valued nature of skin friction relationship near limit.

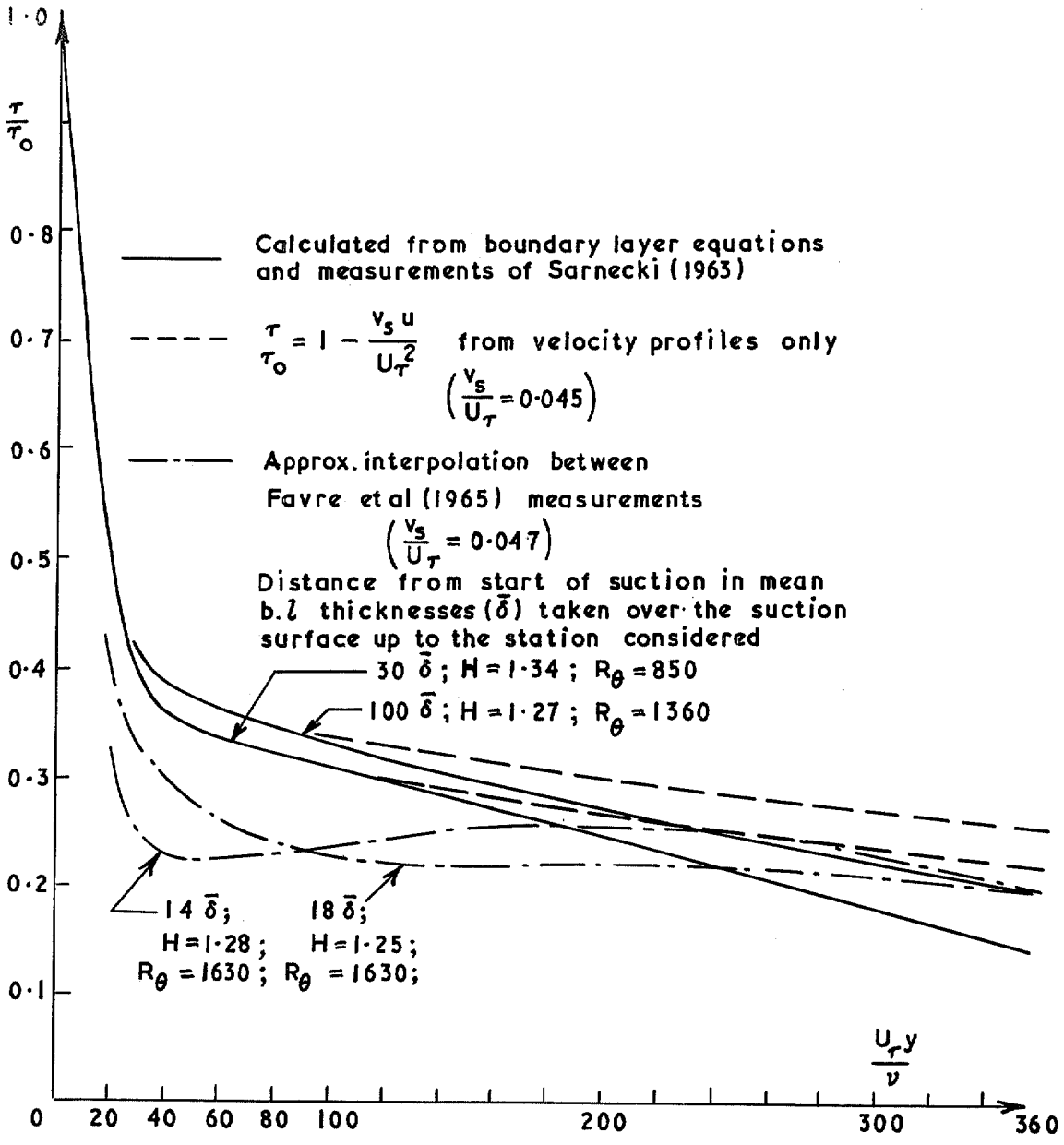

FIG. 28. Comparison of shear stress distributions for $\frac{v_s}{U_1} \approx 0{\cdot}0025$.

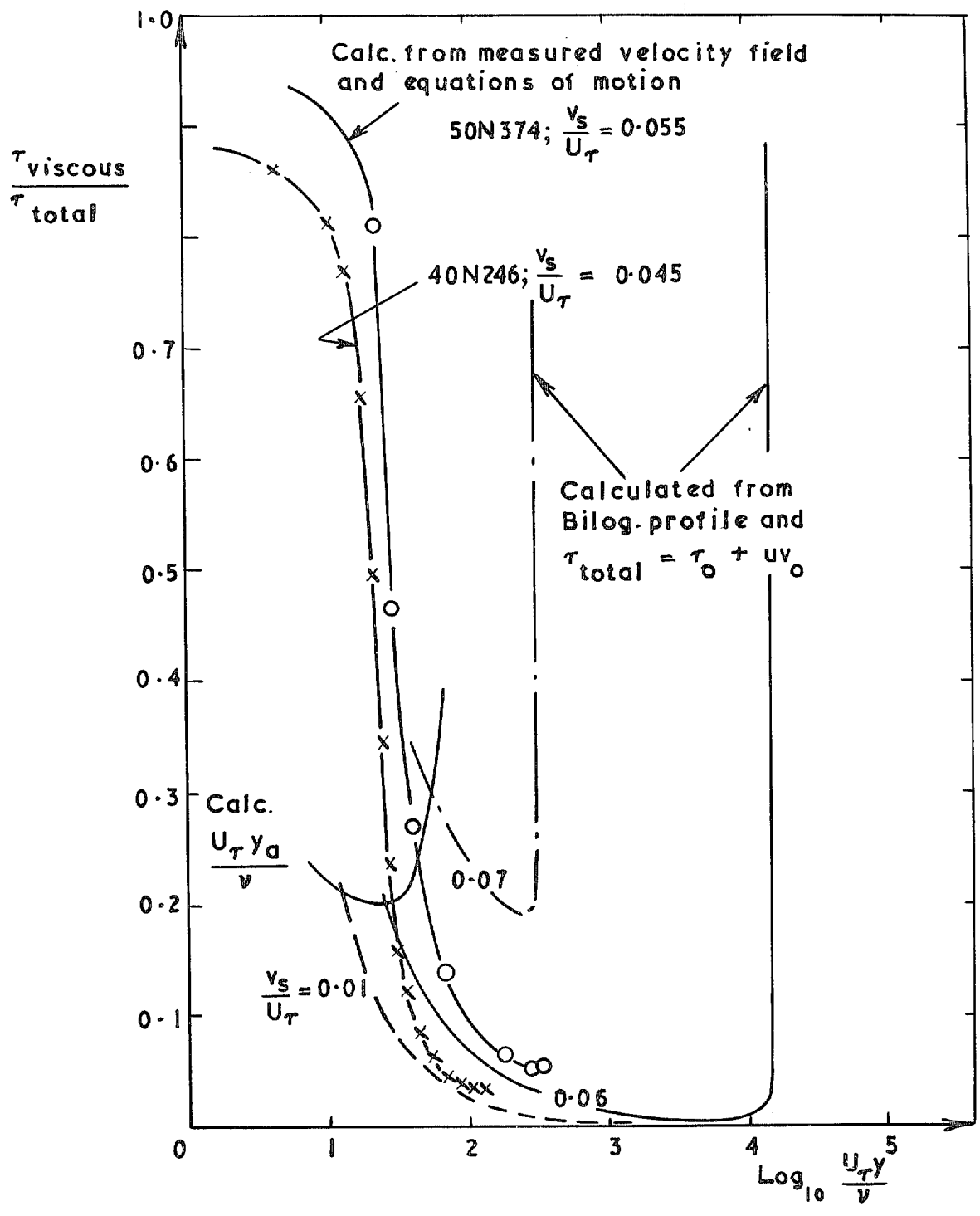

FIG. 29. Test of assumption of fully turbulent flow in the Bilog. region.

Printed in Wales for Her Majesty's Stationery Office by Allens Printers (Wales) Limited
Dd 146916 K5

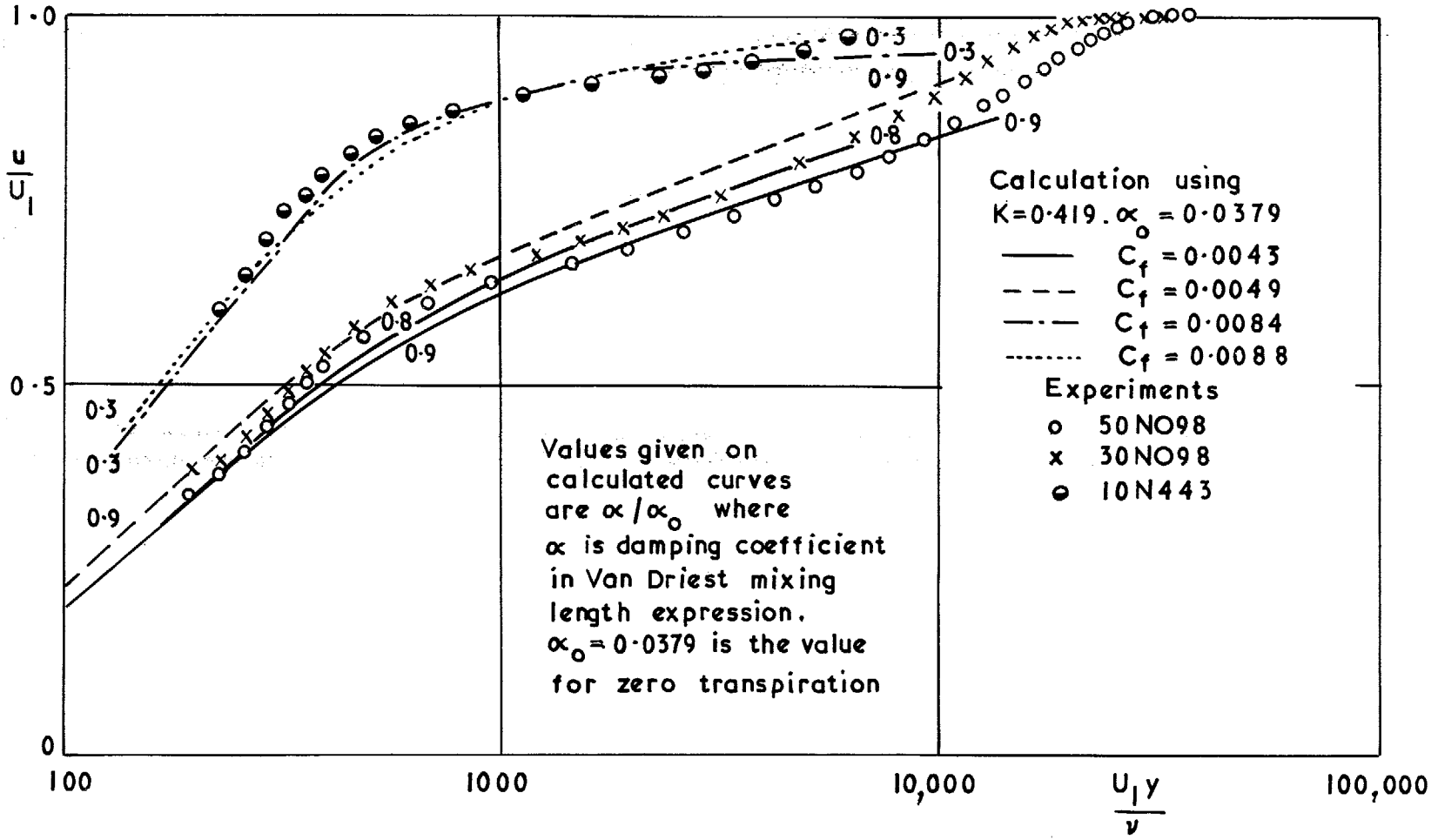

FIG. 30. Comparison of van Driest blending region profiles with experiment.

Published by
HER MAJESTY'S STATIONERY OFFICE

To be purchased from
49 High Holborn, London WC1
13a Castle Street, Edinburgh EH2 3AR
109 St Mary Street, Cardiff CF1 1JW
Brazennose Street, Manchester M60 8AS
50 Fairfax Street, Bristol BS1 3DE
258 Broad Street, Birmingham 1
7 Linenhall Street, Belfast BT2 8AY
or through any bookseller

SBN 11 470322 1